Pergamon

Geochimica et Cosmochimica Acta, Vol. 68, No. 19, pp. 3845-3861, 2004

0016-7037/04 $30.00 + .00

doi:10.1016/j.gca.2004.03.021

# Mg/Ca, Sr/Ca, and stable isotopes in modern and Holocene *Protothaca staminea* shells from a northern California coastal upwelling region

RENEE K. TAKESUE[1,*] and ALEXANDER VAN GEEN[2]

[1]Department of Earth and Environmental Sciences, Columbia University, New York, NY 10025, USA
[2]Lamont-Doherty Earth Observatory of Columbia University, Palisades, New York, NY 10946, USA

(*Received April* 4, 2003; *accepted in revised form March* 18, 2004)

**Abstract**—This study explores the potential of intertidal *Protothaca staminea* shells as high-resolution geochemical archives of environmental change in a coastal upwelling region. Mg/Ca and Sr/Ca ratios were analyzed by excimer laser ablation-inductively coupled plasma mass spectrometry (LA-ICP-MS) at sub-weekly temporal resolution in shells growing ~1 mm per month. Growth patterns of a modern *P. staminea* shell from Humboldt Bay, California, collected in December 1999 made it possible to infer a lifespan from 1993 to 1998. Growth hiatuses in the shell may have excluded records of extreme events. Mg/Ca ratios appeared to be partly controlled by water temperature; the correlation coefficient between temperature and Mg/Ca was $r = 0.71$ in one of four growth increments. Significant year-to-year differences in the sensitivity of Mg/Ca to temperature in *P. staminea* could not be explained, however. Sr/Ca ratios appeared to be more closely related to shell growth rate. Oxygen isotopes, measured at 2-week temporal resolution in the same shell, did not show a clear relation to local temperature in summer, possibly because temperatures were higher and less variable at the King Salmon mudflat, where the shell was collected, than in the main channel of Humboldt Bay, where water properties were monitored. Negative shell $\delta^{13}C$ values ($<-0.5‰$) marked spring and summer coastal upwelling events.

The Mg contents of *P. staminea* midden shells dated to ~3 ka and ~9 ka were significantly lower than in the modern shell. This may have resulted from degradation of a Mg-rich shell organic matrix and precluded quantitative interpretation of the older high-resolution records. Elevated $\delta^{13}C$ values in the ~3 ka shell suggested that the individual grew in highly productive or stratified environment, such as a shallow coastal embayment or lagoon. *Copyright © 2004 Elsevier Ltd*

## 1. INTRODUCTION

Coastal upwelling regions in eastern ocean boundaries are characterized by intense biologic productivity and economically important fisheries (Chavez and Toggweiler, 1995). The ability to predict how climate change will affect productivity in coastal upwelling regions would thus be a valuable tool (Bakun, 1990; Schwing and Mendelssohn, 1997). One approach is to explore how past changes in climate affected coastal upwelling regions. During the solar maximum 11,000 yr ago, northern hemisphere midlatitude insolation was 7% higher than today in summer and 7% lower than today in winter (Kutzbach et al., 1998). An increased summer land-ocean temperature gradient may have resulted in stronger surface winds and intensified coastal upwelling (Kutzbach et al., 1998; Basil and Bush, 2001).

Coastal upwelling results in low water temperatures, high salinity, high nutrients, and increased primary productivity (Huyer, 1983). As marine and estuarine molluscs deposit their shells, trace elements and stable isotopes sensitive to such shifts in water properties may be incorporated into the calcium carbonate lattice, preserving daily records of environmental conditions (e.g., Dodd, 1965; Rhoads and Lutz, 1980). The goal of this study was to explore whether high-resolution geochemical records in modern and Holocene *Protothaca staminea* bivalve shells provided a means to reconstruct environmental change in a region strongly influenced by coastal upwelling.

*P. staminea* is an intertidal bivalve with an aragonite shell and is ubiquitous along the western coast of North America. Its ecology and shell compositional banding, i.e., shell microstructure, are described in detail in the next section. We chose to investigate magnesium to calcium (Mg/Ca) and strontium to calcium (Sr/Ca) ratios in *P. staminea* shells, as well as shell oxygen and carbon stable isotopic compositions ($\delta^{18}O$, $\delta^{13}C$, standard delta notation). Klein et al. (1996a) found a strong positive correlation between Mg/Ca and water temperature in the calcitic layer of *Mytilus trossulus*, suggesting Mg/Ca could be used as a paleotemperature proxy. A similar relationship has not been demonstrated in aragonitic mollusc shells, but cyclic Mg/Ca variations have been observed (Fuge et al., 1993; Toland et al., 2000; Hendry et al., 2001). Some authors, however, have pointed out that Mg incorporation in *Mytilus* sp. appears to be primarily controlled by metabolic processes (Rosenberg and Hughes, 1991; Vander Putten et al., 2000). Early studies of Sr/Ca in mollusc shells also showed apparent relationships with temperature (Dodd, 1965) or salinity (Wolf et al., 1967; Eisma et al., 1976). There is increasing evidence, however, that Sr incorporation into mollusc shells is controlled by metabolic efficiency (Klein et al., 1996b; Purton et al., 1999) or possibly growth rate (Stecher et al., 1996; Vander Putten et al., 2000). A secondary temperature control on physiologic processes could explain apparent correlations between mollusc shell Mg and Sr incorporation and temperature (e.g., Dodd, 1967; Stecher et al., 1996; Toland et al., 2000).

* Author to whom correspondence should be addressed, at U.S. Geological Survey, MS 496, Menlo Park, CA 94025, USA (rtakesue@usgs.gov).

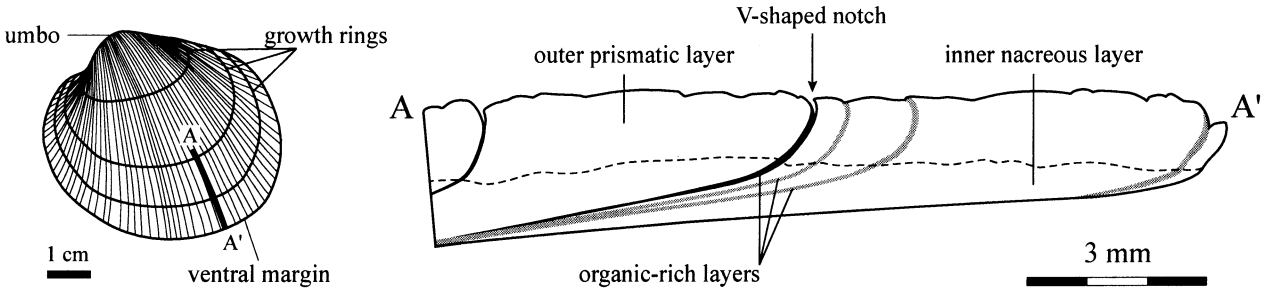


Fig. 1. (left) External view of a *Protothaca staminea* shell (left valve) showing external growth rings. Radial cross section from A to A′ (right) shows shell structural layers, V-shaped notches corresponding to growth bands (black), and organic-rich layers representing growth checks (gray). Dashed line indicates the boundary between the outer prismatic and inner nacreous layers.

Skeletal carbonate oxygen ($\delta^{18}O$) and carbon ($\delta^{13}C$) isotopic compositions have been used as temperature and upwelling tracers (Epstein et al., 1953; Emiliani, 1955; Killingley and Berger, 1979). Many molluscs precipitate their shells in oxygen isotopic equilibrium with ambient water ($\delta^{18}O_w$) (Mook and Vogel, 1968; Grossman and Ku, 1986; Klein et al., 1996b). Grossman and Ku (1986) described the temperature dependence of $^{18}O/^{16}O$ and $^{13}C/^{12}C$ fractionation in aragonitic mollusc shells. In addition, salinity may influence mollusc shell $\delta^{18}O$ and $\delta^{13}C$ in coastal and estuarine environments where freshwater inputs are high (Mook, 1970; Eisma et al., 1976; Krantz, 1990; Jones and Allmon, 1995; Ingram et al., 1996). Mollusc shell $\delta^{13}C$ variations are more difficult to interpret than $\delta^{18}O$ because $^{12}C$-rich metabolically derived carbon may be incorporated into shell carbonate, obscuring variations in the carbon isotope composition of water column dissolved inorganic carbon ($\delta^{13}C_{DIC}$) (Grossman and Ku, 1986; Tanaka et al., 1986; Klein et al., 1996b). When metabolic contributions could be constrained, mollusc shell $\delta^{13}C$ has been used as a coastal upwelling tracer, since $\delta^{13}C_{DIC}$ experiences a nutrient-like surface-to-deep ocean enrichment (Killingley and Berger, 1979; Krantz et al., 1988; Jones and Allmon, 1995). Killingley and Berger (1979) found an average $\delta^{13}C$ depletion of 0.7‰ in southern California mussel shells during the upwelling season. Mollusc shell $\delta^{13}C$ has also been used to identify past productivity events, since photosynthesis enriches surface waters in $^{13}C$ relative to $^{12}C$ (Purton and Brasier, 1997).

The ecology and shell characteristics of the bivalve *Protothaca staminea* are described in Section 2, as well as the sample localities and the specimens used in this study. Environmental data sets, analytical methods, and the procedure for assigning a timescale to the modern *P. staminea* shell are described in Section 3. Humboldt Bay climatology and geochemical variations in *P. staminea* shells are described in Section 4. In Section 5 we discuss relationships between shell geochemistry and environmental variables today, and make some inferences about coastal conditions 3000 and 9000 yr ago. Concluding remarks are given in Section 6.

## 2. SAMPLES

The Pacific littleneck clam *Protothaca staminea* (Fig. 1) was chosen for this study because it was one of three species present at both the modern study site, Humboldt Bay (40.8°N), California, and an early Holocene coastal shell midden at Duncan's Landing (38.4°N), California.

### 2.1. *Protothaca staminea* Ecology

*P. staminea* burrows 5–15 cm below the sediment surface and inhabits intertidal environments ranging from exposed rocky beaches to protected mudflats (Fraser and Smith, 1928). *P. staminea* is a suspension-feeder that consumes all plankton small enough to be ingested, and its growth rate is positively correlated with food availability (Smith, 1928). Geographically, *P. staminea* occurs from Prince William Sound, Alaska, to Baja California, Mexico (Harrington, 1987) where annual water temperature ranges are 1.2–12.5°C and 18.7–26.7°C, respectively. While freshwater runoff does not cause mortality, *P. staminea* is not euryhaline (Paul and Feder, 1973). No studies have reported an upper salinity tolerance for *P. staminea*, however salinity reaches 35 in summer off Baja California. Sexual maturity occurs at the end of the second or third year (Fraser and Smith, 1928; Quayle, 1943). At 60.5°N, Feder et al. (1979) found that females spawned in the month of June. At lower latitudes, spawning occurred earlier and possibly more than once per year (Quayle, 1943).

### 2.2. *Protothaca staminea* Shell Structure and Growth

*P. staminea* shells consist of two aragonitic layers: an outer prismatic layer and an inner nacreous layer (Fig. 1). Shell layers consist of three microstructural elements: inorganic crystalline calcium carbonate, an intracrystalline organic matrix, and extra-crystalline organic layers. Under reflected light organic layers are darker than calcium carbonate. Organic layers form by the dissolution of previously deposited shell (containing intracrystalline organic matrix and calcium carbonate) when valve closure causes the shell-precipitating extrapallial fluid to become acidic. The thickness of an organic layer thus reflects the length of time valves were closed.

Three kinds of dark organic layers were observed in *P. staminea* shells using a reflected light microscope. The first kind of organic layer was tens of microns wide and was associated with an external growth ring that appears as a V-shaped notch in cross-sectional profile (Pannella, 1975; Peterson and Ambrose, 1985) (Fig. 1). This kind of layer will henceforth be referred to as a 'growth band' and indicated by a

numbered capital B, e.g., 'B1' would refer to the first-deposited growth band. Growth bands and external rings form as shell growth slows or stops in response to seasonally decreasing water temperatures, typically in winter (Fraser and Smith, 1928; Paul and Feder, 1973). Peterson and Ambrose (1985) showed that growth bands and corresponding external rings were deposited annually by *P. staminea* living in muddy-sand environments, but sometimes more frequently in higher energy environments. The second kind of organic layer was tens of microns wide and was not associated with a V-shaped notch on the external surface because shell growth stopped abruptly and resumed abruptly in response to a transient environmental or physiologic stress (e.g., storms, extreme temperatures, spawning) (Kennish, 1980). The second kind of organic layer will be called a 'growth check'. The third kind of organic layer was $\leq$10 $\mu$m-wide and formed when *P. staminea* was exposed to air at low tide and closed its valves, interrupting calcium carbonate deposition (Pannella, 1975). When bivalve shells close tightly, a thin layer of organic matter structurally and chemically distinct from the intracrystalline organic matrix is deposited (Pannella, 1975). These tidally deposited layers will henceforth be referred to as 'growth lines'. Since the northern California coast experiences mixed semidiurnal tides, growth lines form once per lunar day during spring tides (Berry and Barker, 1975) and twice per lunar day during neap tides. A neap tide couplet can be distinguished from spring tide lines because one line is fainter and thinner than the other (Evans, 1972).

*P. staminea* grows fastest in its second year, then more slowly as it ages (Fraser and Smith, 1928; Schmidt and Warme, 1969; Paul and Feder, 1973; Harrington, 1987). With decreasing latitude (i.e., increasing temperature, productivity, and daylight hours), *P. staminea* growth rate increases and longevity decreases. The average lifespan of *P. staminea* at the northern California coast is 8 yr (Harrington, 1985).

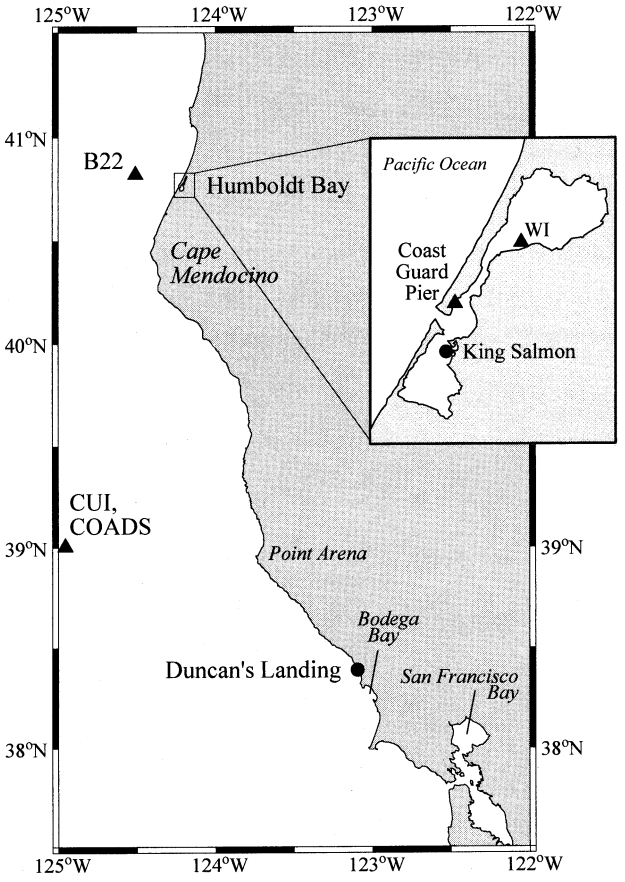


Fig. 2. Northern California map showing locations where *P. staminea* shells were collected (circles) and where climatological parameters were measured (triangles). (B22) Eel River buoy 28 km offshore, (CUI) center of a 300 km square box where the coastal upwelling index was calculated, (COADS) center of a 200 km-square box where solar insolation measurements were averaged, (WI) Woodley Island meteorological station.

### 2.3. Site and Specimen Descriptions

#### *2.3.1. Modern shells*

Humboldt Bay (HB), California, was chosen as the site at which to compare geochemical variations in a *P. staminea* shell to environmental variables because water column nutrients, the nutrient-like trace element cadmium, and salinity, all of which are used as coastal upwelling tracers, were monitored there from March 1994 through August 1998. HB is a shallow (3.5 m deep) semi-enclosed embayment within the Cape Mendocino coastal upwelling system (Fig. 2). No major rivers drain into Humboldt Bay and freshwater inflow from small sloughs and creeks accounts for less than 5% of the daily tidal exchange (Barnhart et al., 1992).

*P. staminea* shells were dug from 10–20 cm below the sediment surface at low tide on December 26, 1999, at the King Salmon mudflats, across from the mouth of HB (Fig. 2). Salinity and major ion concentrations at King Salmon are similar to those on the open coast (Dodd and Crisp, 1982; Barnhart et al., 1992). The mudflat is exposed to air when water level falls 1 m below mean lower low water (MLLW). This site was chosen because live *P. staminea* were harvested here in the past, and it could be accessed without a boat. Unfortunately, no live *P. staminea* were found on the December 1999 sampling date, although empty in-place shells were abundant. A 60 mm-long (not accounting for shell convexity) articulated shell was chosen for high-resolution trace element analysis by laser ablation inductively coupled plasma mass spectrometry (LA-ICP-MS). The shell had a 1-cm wide moon snail (*Polinices* sp.) bore hole on its umbo, suggesting that the clam died in situ due to predation. The Humboldt Bay *P. staminea* shell used for LA-ICP-MS analysis will henceforth be referred to as HB1. A second *P. staminea* shell, henceforth referred to as HB2, was used to determine the Mg content of the oxidizable, presumably organic, shell fraction.

#### *2.3.2. Midden shells*

Holocene-age *P. staminea* shells were obtained from the archive collection of Duncan's Landing Cave site (California Department of Parks and Recreation Site SON-348/H, 240 km south of HB; Fig. 2), the only known shell midden on the northern California coast with early Holocene deposits (Erlandson, 1994). Duncan's Cave presently sits on a small headland on the open coast, but when the shell midden began accumu-

lating approximately 9000 yr ago, sea level may have been up to 25 m lower than today due to greater continental ice volume (Bard et al., 1990; Edwards et al., 1993; Kutzbach and Ruddiman, 1993). A paleo-faunal analysis of midden shellfish remains suggests that the coastal environment changed from protected embayment/lagoon to rocky intertidal as sea level rose through the early and late Holocene (Erlandson, 1994).

The 3 m deep shell midden was deposited inside a rock cave from 9400 ± 450 yr before present (yr BP) to 3240 ± 150 yr BP (Schwaderer et al., 1990; Erlandson, 1994). The lowermost midden stratum was underlain by Pleistocene beach sands, and the uppermost midden stratum was overlain by soil. Only 20% of excavated shells were archived. Eleven whole *P. staminea* valves were present in 7 of 25 strata archives. Permission was obtained to use two *P. staminea* specimens for preliminary geochemical investigations. *P. staminea* valves were selected from the oldest and youngest strata in which they were present, ~9000 yr ago (~9 ka) and ~3 ka, respectively. The specimens collected from the ~9 ka and ~3 ka midden strata will henceforth be referred to as M9 and M3, respectively. Shell M9 was chosen because it was the largest (59 mm-long, not accounting for shell convexity) and best preserved of the two *P. staminea* valves present in the 9 ka stratum archive. Shell M3, 49 mm-long, not accounting for shell convexity, was the only *P. staminea* valve in the 3 ka stratum archive, so it was analyzed even though the exterior surface was not well preserved.

## 3. METHODS

### 3.1. Humboldt Bay Environmental Data Sets

To relate *P. staminea* shell structure and chemistry to environmental conditions, HB water temperature, salinity, precipitation, and coastal upwelling records were compiled for the period 1995–1999.

#### 3.1.1. Water temperature

HB water temperature was measured hourly by a National Oceanic and Atmospheric Administration (NOAA)/National Ocean Service Water Level Observation Network (NOS) sensor mounted on the pier of the HB Coast Guard station (Fig. 2). NOS sensor data were available beginning in October 1993. Daily water temperatures were calculated as 24-h averages. Since only preliminary data were available from NOS, the sensor record was compared to the sea surface temperature record from the NOAA Eel River Buoy 46022 (B22) moored 28 km offshore (Fig. 2). Apparent inaccuracies in the NOS temperature record during March 1–September 27, 1997, October 31–December 1998, and December 21–31, 1999 (see Section 4.1), made it necessary to substitute B22 data for NOS data during these periods. Temperatures at B22 were not always representative of temperatures in Humboldt Bay because strong cross-shore temperature gradients could have occurred within 20 km of the coast during coastal upwelling (Huyer, 1983; Brink and Cowles, 1991; van Geen et al., 2000).

#### 3.1.2. Salinity

Surface water salinity samples were collected near the HB Coast Guard station from March 1994 to August 1998. Sampling frequency was twice a month during summer (March–September) and once a month during winter. Salinity was measured on a Guildline salinometer calibrated with IAPSO (International Association for Physical Science of the Ocean) standard seawater. Salinity, as defined by the 1978 Practical Salinity Scale (PSS-78), is unitless (UNESCO, 1981). This convention is used here.

#### 3.1.3. Climatological parameters

Monthly solar radiation values for 1995 are from the COADS (Comprehensive Ocean-Atmosphere Data Set) climatology at grid point 39°N, 125°W. COADS data are observations by ships at sea averaged over a 200 km × 200 km grid box. Daily Coastal Upwelling Indices (CUI) at 39°N, 125°W, available from the Pacific Fisheries Environmental Laboratory (PFEL), were used to estimate coastal upwelling off Humboldt Bay. Daily CUIs are geostrophic offshore mass transports calculated from surface pressure gradients interpolated over 300 km × 300 km grid boxes (Schwing et al., 1996). Local precipitation records were obtained from the NOAA meteorological station on Woodley Island in Humboldt Bay.

### 3.2. Shell Analyses

Shell valves were sectioned radially along axes of maximum growth using a diamond-tipped table-top band saw. Radial cross sections were polished on diamond-tipped lapping wheels to reveal internal growth bands, then photographed at 200× magnification with a digital camera mounted vertically on a reflected light microscope.

#### 3.2.1. Diagenetic indicators

*3.2.1.1. Mineralogy.* Aragonite is the least-stable calcium carbonate phase at the Earth's surface, and is diagenetically transformed into low-Mg calcite (Land, 1967; Brand and Veizer, 1980). Shell mineralogical analyses, determined by qualitative X-ray Diffraction (XRD), indicated whether diagenetic mineral transformation had occurred. Shell powders for XRD were obtained by drilling into unpolished shell cross sections with a 1.0 mm burr fit to a vertically mounted pedal-activated dremel tool. The dremel was not equipped with a gauge to measure rotation rate. The detection limit of the Philips X'Pert MPD (Multi-Purpose Diffractometer) used for mineralogical analyses was 1–2% by weight.

*3.2.1.2. Manganese content.* When meteoric water alters marine carbonate, manganese (Mn) concentrations may increase (Brand and Veizer, 1980) because meteoric water contains ~40 times more Mn than seawater (Drever, 1997). Mn concentrations (LA-ICP-MS measurements described in the next section) in shells M3 and M9 were compared to Mn concentrations in HB1 as a relative indicator of diagenetic trace element exchange.

#### 3.2.2. LA-ICP-MS

Laser ablation inductively coupled plasma mass spectrometry (LA-ICP-MS) was used for high resolution in situ trace element measurements in the outer prismatic layer of *P. staminea* shells (Fig. 1). The outer prismatic layer was chosen for analysis because its Mg content was five times higher than in the inner nacreous layer. Transects of 90 $\mu$m or 100 $\mu$m-diameter spots spaced at 200 $\mu$m intervals were ablated from the shell ventral (growing) margin toward the umbo.

The laser ablation system at Lamont-Doherty Earth Observatory (LDEO) consisted of an excimer laser (193 nm, manufactured by Lambda Physik) interfaced directly to the torch of a PlasmaQuad 2+ (PQ2+) quadrupole inductively coupled plasma mass spectrometer (manufactured by VG Elemental) via Teflon-lined Tygon tubing. Typical settings for the laser and PQ2+ are shown in Table 1.

*P. staminea* shells were analyzed in 2 years using different instrument configurations. In June 2000, $^{24}$Mg, $^{43}$Ca, $^{55}$Mn, $^{88}$Sr, $^{114}$Cd, and $^{138}$Ba were analyzed in shell HB1 over a two-day period (1–180 spots, 181–279 spots; where 'spot' refers to an ablation site on the shell). At this time the PQ2+ software recorded count intensity data as an average over a 12-s measurement period. Count intensities from three 12-s measurements of the same spot were averaged to obtain count intensities for each spot. One standard deviation for a spot averaged 25%. In summer 2001, $^{11}$B, $^{24}$Mg, $^{27}$Al, $^{29}$Si, $^{31}$P, $^{43}$Ca, $^{55}$Mn, and $^{88}$Sr were analyzed in shells M3 and M9. Shell M3 was analyzed over two days (1–30 spots, 31–120 spots), shell M9 was analyzed on one day (1–180 spots). In 2001 the PQ2+ software recorded count intensities after each 0.6-s mass scan. For each laser spot, count intensities were

Table 1. Excimer laser and ICP-MS settings and system configurations during 2000 and 2001.

| | 2000 | 2001 |
|---|---|---|
| *Laser configuration* | | |
| sample chamber | attached to stage by vacuum | self-contained |
| distance upstream of torch Ar gas introduced | 1 m | 1.4 m |
| *Laser settings* | | |
| energy output | 23 mJ | 78–98 mJ |
| laser firing frequency | 6 Hz | 10 Hz |
| spot size | 100 $\mu$m | 90 $\mu$m |
| *PQ2+ settings* | | |
| data acquisition mode | peak jumping (12-s average) | peak jumping (0.6-s mass scan) |
| tuning mass | $^{127}$I | $^{24}$Mg, $^{43}$Ca |
| mass range | 24–138 (18 masses) | 24–88 (7 masses) |
| number of replicate analyses | 4 | 70 |
| *PQ2+ gas flows* | | |
| Helium flow | 1–1.2 L/min | same |
| Ar auxiliary flow | 0.5–0.7 L/min | same |
| Nebulizer flow | 2–2.2 L/min | same |

measured for 45 s (70 mass scans). Data from the 20–40 s interval (n = 32) were averaged to obtain count intensities for each spot. The 20–40 s interval was chosen because signal intensity leveled off and mass-dependent fractionation was not observed after 20 s. One standard deviation for a spot averaged 5%. Also in 2001, the ablated sample carried in helium was introduced into the ICP-MS carrier gas line 1.4 m upstream of the torch (previously 1.0 m upstream), which increased signal stability.

A silicate glass standard containing trace elements in concentrations of 500 ppm from the National Institute of Standards and Technology (NIST 610) was used to tune the PQ2+ and to correct for instrument drift during each run. A raster pattern translating at 15 $\mu$m per second was ablated during tuning (to masses $^{24}$Mg and $^{43}$Ca simultaneously) to eliminate signal attenuation. Data acquisition was preceded by a background (carrier gas blank) measurement and a 20 s preablation step, which minimized matrix effects between glass and carbonate (Sinclair et al., 1998). Background counts were removed from all element count intensities, and background-corrected values were then ratioed to $^{43}$Ca. A linear drift correction was applied over the sample run to correct for mass-dependent instrument drift when necessary (Sylvester and Ghaderi, 1997).

LA-ICP-MS 1$\sigma$ variability of sequential NIST 610 Mg/Ca and Sr/Ca ratios was 1.5% and 1.3%, respectively (n = 4). Measurement of Mg/Ca and Sr/Ca ratios in an external standard by flame atomic absorption (see next section) gave a 1$\sigma$ variability of 2.9% and 4.3%, respectively (n = 6). Adding these errors, the uncertainties in standardized Mg/Ca and Sr/Ca ratios were 4.4% and 6.6%. All errors associated with average values are reported as $\pm$ 1$\sigma$ (standard deviation of the mean) unless otherwise noted. When testing levels of significance, *p*-values >0.05 were considered not significant.

### 3.2.3. Flame atomic absorption

A major challenge for quantitative analysis by LA-ICP-MS is finding a matrix-matched standard with similar physiochemical properties as the sample material (Perkins et al., 1991; Sinclair et al., 1998). Some studies have found that silicate glass standards are an appropriate reference material for quantitative analysis of carbonates (Feng, 1994; Hendry et al., 2001; Fallon et al., 2002). In our case, however, preliminary laser ablation tests showed very different $^{24}$Mg/$^{25}$Mg and $^{43}$Ca/$^{44}$Ca ratios in NIST 610 glass versus aragonite bivalve shells, indicative of matrix-dependent fractionation in the plasma. We obtained absolute Mg/Ca and Sr/Ca values for *P. staminea* shells by scaling LA-ICP-MS data to Flame Atomic Absorption (AA) measurements of total Mg and Sr normalized to total Ca.

For AA analyses, approximately 1 mg of powder was drilled from the outer prismatic layer of HB1, M3, and M9, collected over weighing paper, then transferred to polypropylene micro-centrifuge vials. Biogenic carbonates are typically subjected to oxidative and reductive cleaning steps before trace element analyses to remove the organic fraction and secondary contaminant phases (Rosenthal et al., 1999). However, to obtain absolute scales for LA-ICP-MS data, AA samples were not cleaned in any way so that their compositions would match ablated shell material as closely as possible. A 1.2 mM lanthanum-oxide ($La_2O_3$) solution in 0.4% hydrochloric and 1% nitric acid was used to dissolve shell powders directly in micro-centrifuge tubes. The $La_2O_3$ solution was also used to dilute samples.

To determine whether the organic fraction contributed to total Mg concentrations measured by LA-ICP-MS, Mg/Ca ratios in HB2 shell powders were subjected to oxidative cleaning, then compared to Mg/Ca ratios in HB2 shell powders that were not cleaned. An oxidizing solution consisting of 100 $\mu$L hydrogen peroxide and 3 mL 0.1 N sodium hydroxide was added to micro-centrifuge vials containing shell powders. Samples were placed in a hot water bath (90°C) for 2 min, transferred to an ultrasonic bath for 30 s, decanted, then rinsed with trace metal-clean water (Milli-Q). These steps were repeated three times. Shell powders were dissolved as described above.

Total Mg, Sr, and Ca were measured on a Hitachi Z8200 Flame Atomic Absorption Spectrophotometer. External matrix-matched consistency standards were run every 12 samples to correct for instrument drift and sample evaporation. Consistency standard Mg/Ca and Sr/Ca ratios varied 2–4% over a run. Each laser ablation transect (ranging from 30–85 spots in length) was scaled by a constant factor that produced the best fit (minimized the sum of squared residuals) between LA-ICP-MS and AA data. Sr/Ca ratios standardized to NIST610 averaged 23 $\pm$ 4% (n = 4) and 10 $\pm$ 7% (n = 3) higher in 2000 and 2001, respectively, than absolute Sr/Ca ratios found by AA. Mg/Ca ratios standardized to NIST610 were both higher and lower than absolute Mg/Ca ratios found by AA, averaging 4 $\pm$ 10% (n = 4) higher in 2000 and 10 $\pm$ 11% (n = 3) lower in 2001.

### 3.2.4. Oxygen and carbon stable isotopes ratio ($\delta^{18}O$ and $\delta^{13}C$) analysis

Following LA-ICP-MS analysis, shell powders were drilled from the shell cross-sectional surface for stable oxygen and carbon isotope analyses using a 0.3 mm or 0.5 mm burr fit to a vertically mounted dremel tool. Sampling resolution was 0.5–1.0 mm along from the ventral margin until the outer prismatic layer narrowed to less than 0.5 mm. Approximately 200 $\mu$g of powder was transferred into borosilicate vials and dried overnight at 60°C. $\delta^{18}O$ and $\delta^{13}C$ were measured at LDEO on a Micromass Optima mass spectrometer equipped with a Multiprep carbonate preparation system. Samples were reacted under vacuum with 85% phosphoric acid at 90°C for 15 min to produce $CO_2$ gas for mass spectrometric analysis. Long-term reproducibility of an internal lab standard was $\pm$0.07‰ for $\delta^{18}O$ and $\pm$0.05‰ for $\delta^{13}C$ (J. Lynch-Stieglitz, pers. comm.). Values are given in standard delta notation relative to the Vienna PeeDee Belemite (VPDB) standard.

When comparing HB1 shell $\delta^{13}C$ values with M3 and M9 $\delta^{13}C$ values, a $-0.6 \pm 0.2$‰ anthropogenically induced shift in surface ocean $\delta^{13}C_{DIC}$ predicted by Ortiz et al. (2000) was taken into account. When comparing M9 shell $\delta^{18}O$ values with HB1 $\delta^{18}O$ values, a $+0.2$‰ shift in mean ocean $\delta^{18}O$ due to increased continental ice volume was taken into account, assuming sea level was 25 m lower than today at ~9 ka (Bard et al., 1990; Edwards et al., 1993) and that the magnitude of the mean ocean $\delta^{18}O$ shift was 1‰ (Schrag et al., 1996).

### 3.3. Shell Chronologies

Shell microstructural elements were identified under 200× magnification on freshly cut and polished radial cross sections of HB1, M3, and M9. Relative shell chronologies, or numbers of years of growth, were determined based on the assumption that V-shaped external growth rings corresponding to dark internal growth bands were deposited annually. This assumption was valid for HB1, since it grew in a muddy low-energy environment.

To allow a direct comparison between shell chemistry and environmental or climatological conditions, an absolute chronology was assigned to HB1 using shell growth features. Since HB1 was not collected alive, the calendar years during which the shell grew could not be known with absolute certainty. However, a grain of sand incorporated into the sixth growth band (B6) provided a possible starting point. The presence of sediment within a mollusc shell is indicative of storm activity (Kennish, 1980). California's stormiest winter of the last decade was the winter of 1997–1998, during which a strong El Niño event occurred (Ryan et al., 1999). To fix the shell record in time, B6 was positioned in mid-February 1998 at the height of the El Niño storm season. The remaining growth bands were spaced at 1-yr intervals and aligned with the first winter or spring occurrence of water temperatures less than 10.5°C persisting for more than two days. For simplicity, constant growth rates were applied over growth increments. Next, the position of B5 was adjusted so the length of time represented by the sixth growth increment (I6) approximately equaled the number of daily growth lines in that increment. Lunar-day growth lines in I6 could be counted in reflected-light photographs because they appeared as dark brown, <10 $\mu$m-thick lines within a lighter calcium carbonate matrix, and because growth lines were far enough apart throughout I6 to be individually identified. Finally, B3 and B4 were moved 1 yr forward in time and a growth rate equivalent to that in I6 was applied to I7.

## 4. RESULTS

### 4.1. Humboldt Bay Climate, Salinity, and Temperature

Near-normal climatological conditions prevailed in 1995 (Schwing et al., 2002). Salinity and temperature patterns during this year were therefore taken to be representative of the typical seasonal cycle (Fig. 3). From January through May, HB salinity varied between 25.6 and 32.3 with a mean of 30.4 ± 2.0 (1$\sigma$, n = 8). During summer (June–November) salinity was near-constant, averaging 33.4 ± 0.2 (1$\sigma$, n = 9). HB water temperatures did not follow seasonal changes in solar radiation or air temperature, but varied from month to month (Fig. 3). Coldest waters (10–11°C) were present at the coast following strong and persistent upwelling-favorable conditions in April and June. Waters were warmest (13–14°C) in July and September following periods when upwelling-favorable winds weakened (Fig. 3). Winter temperatures, 12–13°C, were intermediate between upwelling and nonupwelling periods.

Apparent temperature extremes in the NOS sensor record during March 1–September 27, 1997 (4–8°C), October 31–December 4, 1998 (17–28°C), and December 21–31, 1999 (14–17°C), were seasonally anomalous and were not mirrored in the B22 temperature record. It seems likely that the NOS sensor experienced calibration errors during these periods,

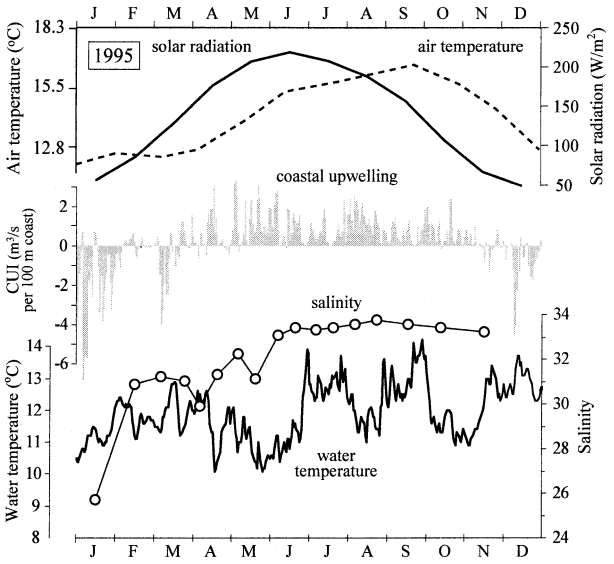


Fig. 3. COADS offshore surface solar radiation (upper solid line), coastal upwelling intensity (gray columns), Humboldt Bay salinity (open circles), and Humboldt Bay water temperature (lower solid line) during 1995. Also shown for comparison are Humboldt Bay maximum daily air temperatures averaged by month for the period 1940–1977 (dashed line), after Figure 2.5 of Barnhart et al. (1992). Positive CUI values indicate coastal upwelling and generally correspond to periods of salinity >33 and reduced water temperatures.

however NOS does not have a maintenance log by which to verify this. Nevertheless, NOS temperatures were replaced by B22 sea surface temperatures when NOS temperatures differed from B22 temperatures by >1°C during these periods. In 1996 and 1998 seasonal temperature patterns were similar to the normal climatology (Fig. 4). Unusually warm conditions, 5°C higher temperatures than in any other year, occurred in September 1997 during a strong El Niño event. In every year, 1 month of low water temperatures occurred in late spring or early summer.

### 4.2. Geochemical Variations in *P. staminea* Shells

#### *4.2.1. Shell HB1*

*4.2.1.1. Shell mineralogy, growth, and manganese content of HB1.* HB1 was composed of aragonite. It had 2 faint juvenile growth bands and 5 strong growth bands (B). Increment (I) length decreased with organism age except in I6, which was shorter than expected (Table 2). Including the last-deposited growth increment, four complete growth increments were analyzed in HB1. Mn concentrations reported here are semiquantitative, since LA-ICP-MS data were standardized to NIST 610 rather than a matrix-matched carbonate standard. Mn concentrations in HB1 ranged from 2 ppm to 11 ppm and averaged 6 ± 2 ppm.

*4.2.1.2. Mg/Ca and Sr/Ca in HB1.* Mean Mg/Ca in HB1 was 2.7 ± 0.4 mmol/mol (n = 279; Fig. 5) and ranged from 1.4 to 3.8 mmol/mol (Table 2). Mean Sr/Ca in HB1 was 2.1 ± 0.4

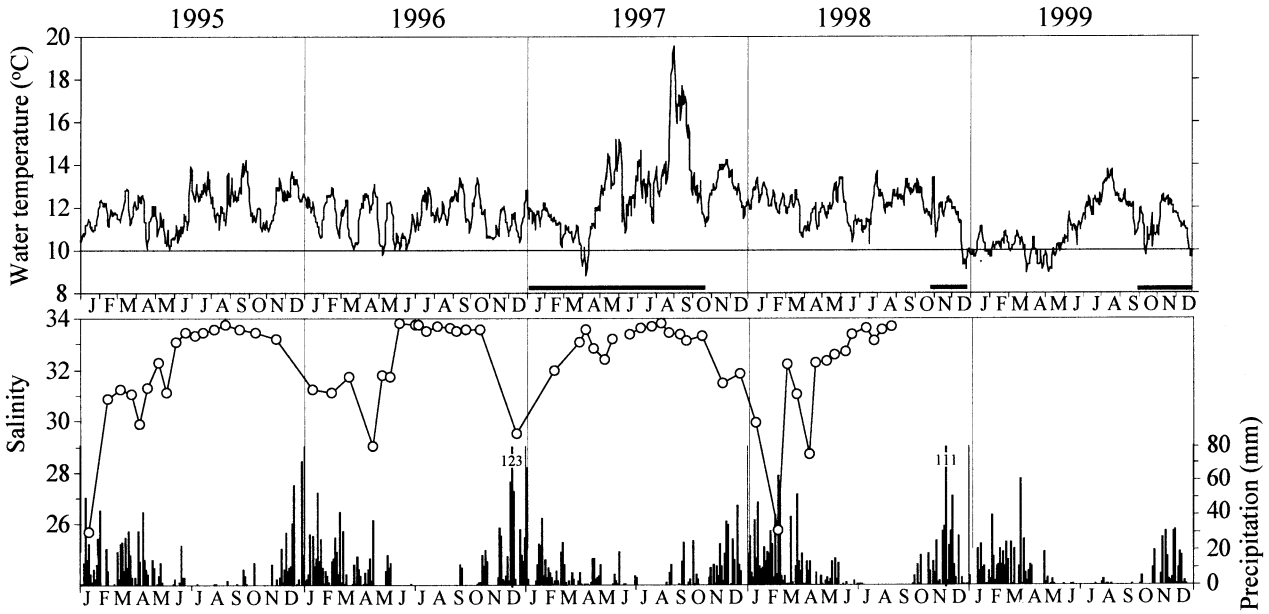


Fig. 4. (upper panel) Composite daily water temperature record with data from the NOS Humboldt Bay sensor and the B22 coastal buoy. Horizontal bars indicate where B22 data were used. Horizontal line drawn at 10°C. (lower panel) Humboldt Bay salinity near the north spit Coast Guard station (open circles) and precipitation at the Woodley Island meteorological station (columns). Numbers on precipitation graph indicate off scale magnitudes of two winter storms.

mmol/mol (n = 279; Fig. 5) and ranged from 1.2 to 3.1 mmol/mol (Table 2). Mg and Sr were highly correlated throughout HB1 (r = 0.82, $p < 0.001$; Fig. 6). In each growth increment, Mg/Ca and Sr/Ca ratios were highest mid-increment and lowest near dark growth bands at the end of each increment (Fig. 6). Sr/Ca minima coincided with Mg/Ca minima in B5 and B6 while Sr/Ca minima preceded Mg/Ca minima by 1–2 mm at B3 and B4. Abrupt decreases in Mg/Ca and Sr/Ca occurred across B3 and B5. There was a general decrease of within-increment mean Sr/Ca with increasing organism age, i.e., an ontogenetic decrease, but not of Mg/Ca (Fig. 5, Table 2).

*4.2.1.3. Stable isotopes ($\delta^{18}O$, $\delta^{13}C$) in HB1.* Average $\delta^{18}O$ in HB1 was 0.6 ± 0.4‰ (n = 79) and ranged from −0.5 to 1.2‰ (Fig. 7; Table 2). In three of five increments, the most negative $\delta^{18}O$ values occurred at the growth band (Fig. 6). At B6 and B7 negative-most $\delta^{18}O$ values coincided with Mg/Ca and Sr/Ca minima. The $\delta^{18}O$ mode value, 0.6‰, the value that occurred most frequently, occurred mid-increment where $\delta^{18}O$ was near-constant, varying 0.1‰ or less (Fig. 6). In I4 this corresponded to the region 34.5–37 mm from the ventral margin, in I5, 19–24 mm from the ventral margin, and in I7, 4–6.5 mm from the ventral margin. High positive correlations were significant ($p \ll 0.001$) between $\delta^{18}O$ and Mg/Ca (r = 0.73) and $\delta^{18}O$ and Sr/Ca (r = 0.65).

The average $\delta^{13}C$ value of HB1, −0.2 ± 0.0‰ (n = 79), was the lowest of the three shells (Fig. 7). HB1 $\delta^{13}C$ ranged from −0.9 to 0.2‰ (Table 2). Shell $\delta^{13}C$ varied cyclically with a saw-toothed pattern in I2, I3, I4, and I5 (Fig. 6). Abrupt decreases to negative-most $\delta^{13}C$ values were followed by gradual increases toward zero. There were no significant relationships between $\delta^{13}C$ and $\delta^{18}O$, Mg/Ca, or Sr/Ca.

*4.2.2. Shell HB2*

Mg was the only trace element measured in HB2. Mg/Ca ratios in uncleaned HB2 powders averaged 1.9 ± 0.2 mmol/mol (n = 36). Mg/Ca ratios in HB2 powders subjected to oxidative cleaning averaged 1.0 ± 0.1 mmol/mol (n = 31).

*4.2.3. Shell M3*

*4.2.3.1. Shell preservation, growth, and diagenetic indicators in M3.* Shell M3 was composed of aragonite. Sectioning, polishing, and microscope examination revealed that several millimeters of the outer prismatic layer were missing from increments 1–7. M3 had 10 growth bands that were easily recognized on the eroded shell surface as topographic ridges of material that was less friable than calcium carbonate. Increment length decreased from I1 to I5, increased at I6, then decreased again through I11 (Table 2). Excluding the last-deposited growth increment, five complete growth increments were analyzed in M3. Data from I11 have been excluded because LA-ICP-MS analyses were not in the outer prismatic layer. One data point (I10) had a manganese concentration greater than the highest Mn concentration in HB1 (11 ppm). When this data point was excluded, the average Mn concentration in M3 (2.88 ± 0.90 ppm) was less than the average Mn concentration in HB1 (5.74 ± 1.55 ppm).

*4.2.3.2. Mg/Ca and Sr/Ca in M3.* Mean Mg/Ca in M3, 1.6 ± 0.4 mmol/mol (n = 107; Fig. 5), was 40% lower than in the modern shell, while the range, from 0.3 to 2.4 mmol/mol, was the same (Table 2). The Sr/Ca mean and range, 1.6 ± 0.3 mmol/mol (n = 107; Fig. 5) and from 0.9 to 2.4 mmol/mol,

Table 2. Trace element (Mg/Ca and Sr/Ca ratios) and stable isotope ($\delta^{18}O$, $\delta^{13}C$) means, standard deviations, ranges, and number of analyses in each increment (I) and in whole shells (ALL).[a]

| | Length (mm) | Mg/Ca (mmol/mol) | | | Sr/Ca (mmol/mol) | | | | $\delta^{18}O$ (‰) | | | $\delta^{13}C$ (‰) | | | |
|---|---|---|---|---|---|---|---|---|---|---|---|---|---|---|---|
| | | Mean | 1$\sigma$ | Range | Mean | 1$\sigma$ | Range | n | Mean | 1$\sigma$ | Range | Mean | 1$\sigma$ | Range | n |
| *Humboldt Bay shell (HB1)* | | | | | | | | | | | | | | | |
| I1 | 8 | | | | | | | | | | | | | | |
| I2 | 13 | | | | | | | | | | | | | | |
| I3* | 22 | 2.9 | 0.2 | 0.8 | 2.4 | 0.2 | 1.0 | 37 | 0.5 | 0.3 | 1.1 | −0.2 | 0.2 | 0.4 | 19 |
| I4 | 17 | 3.0 | 0.3 | 1.2 | 2.4 | 0.3 | 1.5 | 98 | 0.8 | 0.2 | 0.9 | −0.2 | 0.2 | 1.0 | 28 |
| I5 | 14 | 2.7 | 0.3 | 1.2 | 2.2 | 0.3 | 1.3 | 74 | 0.6 | 0.2 | 0.6 | −0.4 | 0.3 | 1.1 | 14 |
| I6 | 6 | 2.0 | 0.3 | 0.9 | 1.6 | 0.2 | 0.6 | 31 | 0.1 | 0.3 | 1.1 | −0.3 | 0.1 | 0.4 | 8 |
| I7 | 7 | 2.3 | 0.4 | 1.4 | 1.7 | 0.3 | 1.0 | 39 | 0.3 | 0.4 | 1.1 | −0.3 | 0.3 | 0.9 | 10 |
| All | 86 | 2.7 | 0.4 | 2.3 | 2.1 | 0.4 | 1.9 | 178 | 0.6 | 0.4 | 1.7 | −0.2 | 0.2 | 1.1 | 79 |
| *Midden shell (M3)* | | | | | | | | | | | | | | | |
| I1 | 17 | | | | | | | | | | | | | | |
| I2 | 10 | | | | | | | | | | | | | | |
| I3 | 8 | | | | | | | | | | | | | | |
| I4* | 5 | 2.1 | 0.2 | 0.9 | 1.9 | 0.2 | 0.7 | 14 | | | | | | | |
| I5 | 3 | 1.5 | 0.3 | 1.3 | 1.6 | 0.3 | 1.0 | 21 | | | | | | | |
| I6 | 5 | 1.6 | 0.2 | 0.7 | 1.6 | 0.2 | 0.6 | 21 | | | | | | | |
| I7 | 4 | 1.8 | 0.3 | 1.0 | 1.7 | 0.3 | 0.8 | 11 | | | | | | | |
| I8 | 3 | 1.6 | 0.6 | 1.8 | 1.4 | 0.2 | 0.7 | 11 | 0.3 | 0.3 | 0.6 | 1.8 | 0.2 | 0.5 | 3 |
| I9 | 2 | 1.6 | 0.4 | 1.2 | 1.5 | 0.2 | 0.7 | 15 | 0.4 | 0.3 | 0.6 | 1.4 | 0.0 | 0.0 | 4 |
| I10 | 2 | 1.5 | 0.4 | 1.5 | 1.6 | 0.2 | 0.7 | 14 | 0.3 | 0.3 | 0.6 | 1.9 | 0.2 | 0.5 | 2 |
| I11 | 2 | | | | | | | | | | | | | | |
| All | 59 | 1.6 | 0.4 | 2.2 | 1.6 | 0.3 | 1.4 | 107 | 0.4 | 0.3 | 0.8 | 1.6 | 0.3 | 0.7 | 9 |
| *Midden shell (M9)* | | | | | | | | | | | | | | | |
| I1 | 7 | | | | | | | | | | | | | | |
| I2 | 21 | | | | | | | | | | | | | | |
| I3* | 12 | 1.2 | 0.1 | 0.1 | 2.6 | 0.2 | 0.4 | 5 | | | | | | | |
| I4 | 19 | 1.1 | 0.1 | 0.6 | 2.6 | 0.2 | 1.1 | 0 | | | | | | | |
| I5 | 5 | 0.9 | 0.1 | 0.3 | 2.0 | 0.3 | 1.3 | 23 | 0.0 | 0.2 | 0.5 | 0.5 | 0.2 | 0.5 | 6 |
| I6 | 13 | 1.0 | 0.2 | 1.0 | 1.9 | 0.4 | 1.4 | 41 | 0.0 | 0.3 | 1.0 | 0.5 | 0.3 | 1.0 | 11 |
| I7* | 10 | 0.8 | 0.2 | 0.8 | 1.8 | 0.2 | 0.8 | 19 | 0.1 | 0.5 | 1.1 | 0.6 | 0.5 | 1.1 | 4 |
| All | 86 | 1.0 | 0.2 | 1.1 | 2.2 | 0.4 | 1.8 | 88 | 0.0 | 0.3 | 1.1 | 0.5 | 0.3 | 1.1 | 21 |

[a] Rounding may have caused ranges here to differ from values given in text. Increment lengths were measured along shell curvature and thus appeared longer here than reported in the text. Asterisks (*) indicate where measurents did not span the entire increment.

respectively, were both ~28% lower than in HB1 (Table 2). Mg and Sr were highly correlated throughout M3 ($r = 0.76$, $p < 0.001$; Fig. 8). In I8, I9, and I10, Mg/Ca and Sr/Ca were highest mid-increment and lowest near dark growth bands (Fig. 8), similar to patterns observed in HB1. Mg/Ca values in I8 and I9 had only one maximum per increment. There were no ontogenetic trends in mean Mg/Ca or Sr/Ca in M3, nor trends in within each increment (Fig. 8; Table 2).

*4.2.3.3. Stable isotopes ($\delta^{18}O$, $\delta^{13}C$) in M3.* Stable isotope measurements in M3 could only be made in I8, I9, and I10 because the outer prismatic layer of other increments was too narrow to sample. There were too few measurements to interpret within-increment variability (Fig. 8). M3 had a similar $\delta^{18}O$ mean ($0.4 \pm 0.3$‰, $n = 9$) as HB1, but a smaller range, from 0.0 to 0.7‰ (Fig. 7, Table 2). Shell M3 had the highest mean $\delta^{13}C$ value of the three shells, $1.6 \pm 0.3$‰ ($n = 9$), and the smallest range, from 1.3 to 2.0‰ (Fig. 7, Table 2). The mean $\delta^{13}C$ value of M3 was 1.2‰ higher than that of HB1 after correction for the anthropogenically induced shift in water column $\delta^{13}C_{DIC}$.

### 4.2.4. Shell M9

*4.2.4.1. Shell preservation, growth, and diagenetic indicators in M9.* M9 was composed of aragonite. The surface of M9 was physically well preserved, however the interior shell surface was darkened, as if from smoke, and the exterior shell surface had two white spots 1 cm in diameter with diffuse borders (the shell itself was salmon-colored). M9 had 2 juvenile growth bands and 4 strong growth bands. Including the last-deposited growth increment, four complete growth increments were analyzed in M9. Twenty two spots throughout M9 had Mn concentrations greater than 11 ppm. Of these, all but two were below 40 ppm Mn. The two highest Mn values in M9 occurred 17.0 mm (Mn = 660 ppm) and 34.6 mm (Mn = 352 ppm) from the ventral margin. Excluding the two highest values, the

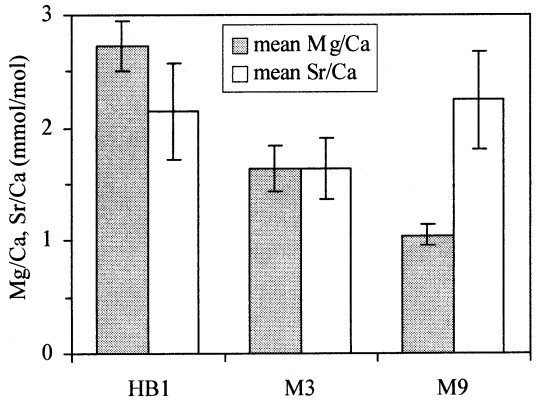


Fig. 5. Mean Mg/Ca (gray) and Sr/Ca (white) in shells HB1, M3, and M9. Error bars indicate one standard deviation of the mean ($1\sigma$).

average Mn concentration in M9 (5.84 ± 6.43 ppm) was statistically indistinguishable from that of HB1.

*4.2.4.2. Mg/Ca and Sr/Ca in M9.* Mean Mg/Ca in M9, 1.0 ± 0.2 mmol/mol (n = 171; Fig. 5), was 59% lower than in HB1, while the range, from 0.4 to 1.5 mmol/mol, was 48% lower (Table 2). The Sr/Ca mean and range, 2.2 ± 0.4 mmol/mol (n = 171; Fig. 5) and from 1.2 to 3.2 mmol/mol, respectively, were the same as in HB1 (Table 2). There were no consistent patterns of Mg/Ca variation within any increment or over the length of M9 (Fig. 9). Sr/Ca ratios, in contrast, varied in a regular sinusoidal manner throughout increments 5–7, despite large spot-to-spot variations in I6 (Fig. 9). In I5-I7, Sr/Ca maxima occurred in the first half of the increment and minima in the second half of the increment. The mean Sr/Ca of each increment decreased with increasing age of the organism (Fig. 9; Table 2).

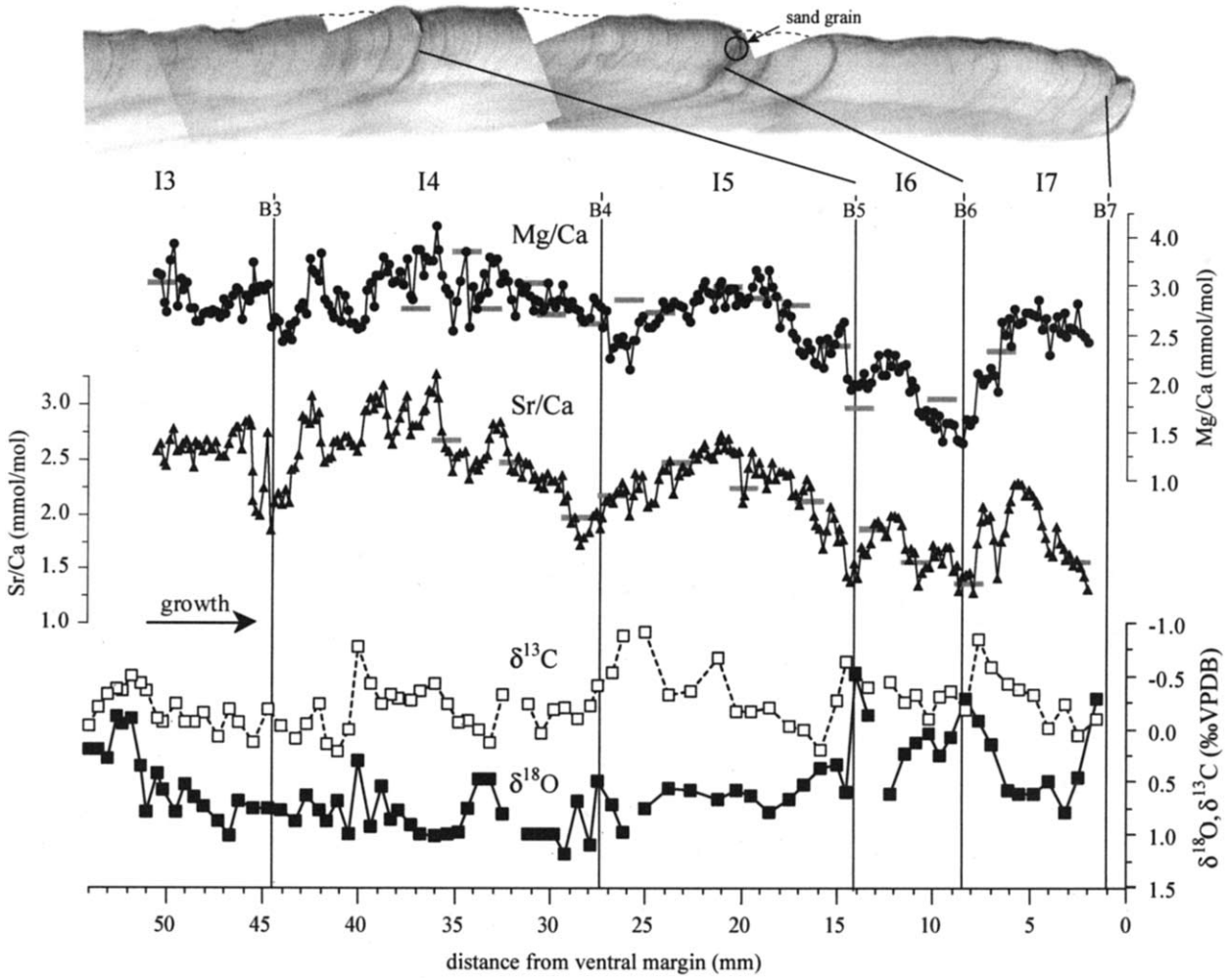


Fig. 6. Cross-sectional photograph and Mg/Ca, Sr/Ca, $\delta^{13}C$, and $\delta^{18}O$ profiles of shell HB1 plotted against distance from the ventral margin. Stable isotopes are plotted on a reversed scale to emphasize warm and fresh conditions. Vertical lines show where growth bands (B) separate growth increments (I). Horizontal gray bars on Mg/Ca and Sr/Ca plots show absolute Mg/Ca and Sr/Ca ratios determined by flame atomic absorption. Arrow indicates direction of growth. Dashed line on cross-sectional photo indicates unphotographed external shell surface. A sand grain incorporated into B6 is circled.

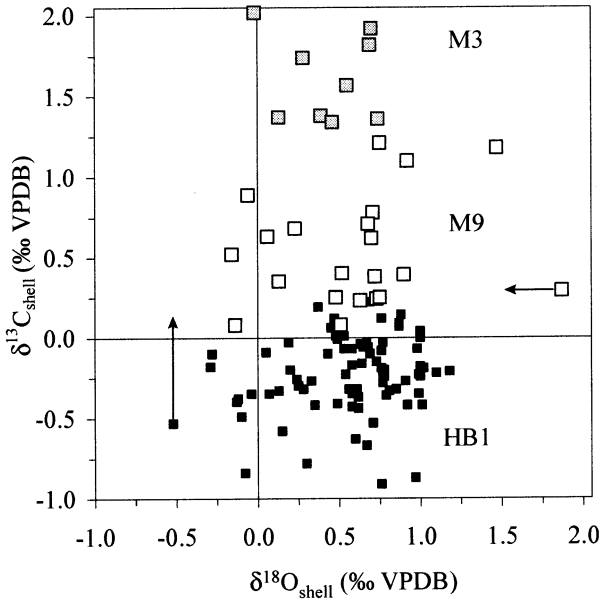


Fig. 7. Plots of $\delta^{13}C$ vs. $\delta^{18}O$ in HB1 (black squares), M3 (gray squares), and M9 (open squares). Vertical arrow indicates the magnitude of a 0.6‰ anthropogenically induced shift in modern surface ocean $\delta^{13}C_{DIC}$ predicted by Ortiz et al. (2000). Left-pointing arrow indicates the magnitude of a 0.2‰ shift in mean ocean $\delta^{18}O$ due to increased continental ice volume at ~9 ka.

*4.2.4.3. Stable isotopes ($\delta^{18}O$, $\delta^{13}C$) in M9.* M9 had the same mean $\delta^{18}O$ value as HB1, 0.6 ± 0.5‰ (n = 21), and a similar range, from −0.2 to 1.9‰ (Fig. 7; Table 2). The small adjustment for ice volume did not affect this result. The two positive-most $\delta^{18}O$ values in M9, 1.5‰ (I4) and 1.9‰ (I5), were the highest $\delta^{18}O$ values observed in any of the shells (Fig. 7). In I3, I4, and I5, the negative-most $\delta^{18}O$ values coincided with Sr/Ca minima (Fig. 9), but the overall relationship between $\delta^{18}O$ and Sr/Ca was not significant. Average $\delta^{13}C$ in M9 was 0.5 ± 0.3‰ (n = 21) and the range was from 0.1 to 1.2‰ (Fig. 7; Table 2). After correcting for the anthropogenically induced surface ocean $\delta^{13}C_{DIC}$ shift, mean shell $\delta^{13}C$ of M9 was indistinguishable from that of HB1. Shell $\delta^{13}C$ did not show consistent patterns within growth increments (Fig. 9).

### 4.3. HB1 Chronology and Growth Rates

According to the preliminary HB1 chronology, HB1 would have grown from 1992 to 1998, and geochemical profiles would have spanned the period from late 1993 to 1998 (Fig. 10a). Two growth checks in I7 could be consistent with two periods of coastal upwelling in April 1998 and June–July 1998 when water temperature decreased abruptly for an extended period. The most negative $\delta^{13}C$ values of each increment would have occurred in March, April, or May, but would have coincided with both warm and cold conditions.

Two growth features were taken to indicate that I6 represented a shorter period of time than other increments. First, I6 had 130 daily growth lines and 15 minor growth checks two or three growth lines-wide. Thus, daily growth banding suggested that I6 represented 4 to 6 months of growth, even allowing for an under-counting of 15 daily growth lines equivalent to one fortnightly tidal cycle. Second, if I6 had grown for an equivalent number of months as I4, its growth rate would have been almost 50% lower than that of I4. When the timescale of I6 was adjusted to represent ~4 months of growth in the second HB1 chronology, the growth rate of I6 was equal to that of I4. Geochemical profiles spanned mid-1995 to 1998, and every $\delta^{13}C$ value less than −0.5‰ coincided with a relative temperature decrease (Fig. 10b).

### 4.4. Environmental Conditions and Geochemical Variations in HB1

#### *4.4.1. Mg/Ca and temperature*

When HB1 Mg/Ca ratios were shown on a chronological timescale, visual inspection revealed similarities between Mg/Ca and HB water temperatures in I4 (Fig. 11). Highest Mg/Ca ratios occurred when waters were warmest. Mg/Ca decreases coincided with temperature decreases in June and August 1996. Despite these apparent similarities, correlations between Mg/Ca and temperature were only moderate ($r = 0.45$, $p < 0.001$) in I4. The standard error for temperatures calculated from the Mg/Ca-temperature regression was 1.2°C, and the regression equation was: Mg/Ca (mmol/mol) = 0.16 ± 0.06 × T (°C) + 1.18 ± 0.70 (95% confidence intervals). When the timescale of I4 was fine-tuned so that similar features of the Mg/Ca profile and temperature records aligned (six additional tie-points, Fig. 12), the correlation between shell Mg/Ca and temperature improved ($r = 0.71$) and the standard error of the Mg/Ca-temperature regression decreased to 0.7°C. The equation describing the fine-tuned relationship between shell Mg/Ca and temperature in I4 is: Mg/Ca (mmol/mol) = 0.23 ± 0.05 × T (°C) + 0.35 ± 0.52 (95% confidence intervals). The fine-tuned relationship was used as the modern calibration.

#### *4.4.2. Sr/Ca and temperature*

There was a moderate correlation between Sr/Ca ratios and HB water temperature in I4 and ($r = 0.49$, $p < 0.001$), but the correlation did not improve significantly when the I4 timescale was fine-tuned ($r = 0.52$, Fig. 12). On the two occasions when late winter Sr/Ca minima preceded Mg/Ca minima, i.e., early March 1996 (before B3) and late February 1997 (before B4), increases in Sr/Ca coincided with a brief cold period (Fig. 5).

#### *4.4.3. Shell $\delta^{18}O$ and $\delta^{13}C$ variations with respect to salinity and temperature*

When salinity was nearly constant in summer and fall, one might expect shell $\delta^{18}O$ to reflect changes in water temperature. If the timescale for HB1 is correct, this was generally not the case. Only from April through September 1997 did shell $\delta^{18}O$ show a negative covariance with temperature (Fig. 11). During low salinity (<32) rainfall runoff events in winter (Fig. 4), one might expect shell $\delta^{18}O$ to decrease even if low water temperatures partially offset the magnitude of this decrease. Only in February 1998 did the local $\delta^{18}O$ minimum coincide with salinity <32.

According to the shell chronology, the four most negative $\delta^{13}C$ values in HB1 were recorded when waters were relatively

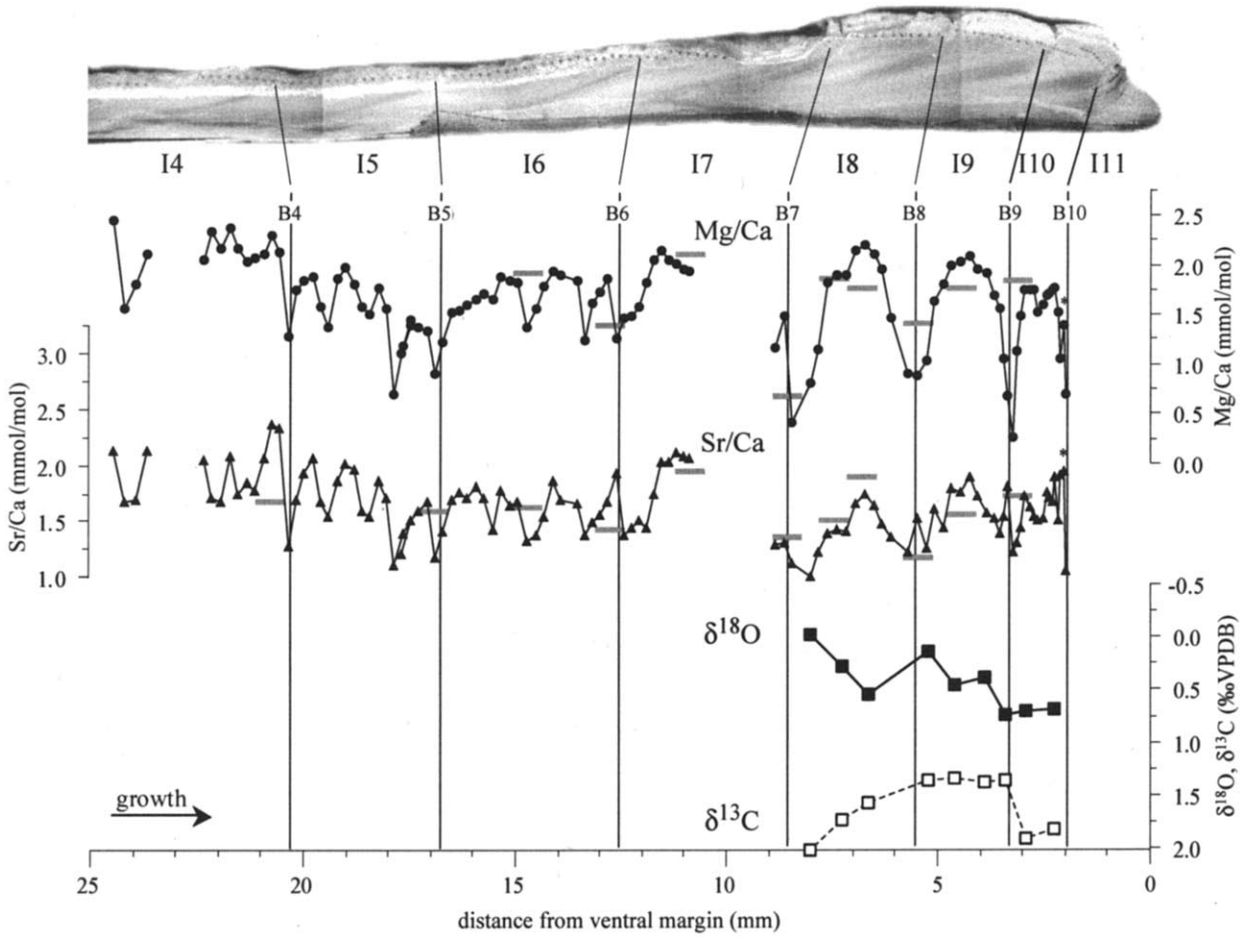


Fig. 8. Cross-sectional image and Mg/Ca, Sr/Ca, $\delta^{18}O$, and $\delta^{13}C$ profiles in shell M3 plotted against distance from the ventral margin. Stable isotopes are plotted on a reversed scale to emphasize warm and fresh conditions. Vertical lines show where growth bands (B) separate growth increments (I). Horizontal gray horizontal bars on Mg/Ca and Sr/Ca plots show absolute Mg/Ca and Sr/Ca ratios determined by flame atomic absorption. Asterisk (*) indicate laser spot with Mn >11 ppm. Laser ablation craters are visible along the upper edge of the shell.

cold: June 1996, March 1997, October 1997, and April 1998. Only three of these occurrences were independent results, since the position of B6 (and the preceding negative $\delta^{13}C$ value) was specified. Negative $\delta^{13}C$ values following B3 and B4 coincided with the earliest occurrence of salinity >33.

### 4.4. Past Temperature Estimates from Mg/Ca

Although Mg/Ca ratios in HB1 did not as a rule appear related to temperature, Mg/Ca variations in the last three increments of M3 resembled seasonal changes in solar radiation (Fig. 3). Mean Mg/Ca ratios were 40% lower in M3 and 59% lower in M9 than in HB1, however, and temperature minima calculated for M3 and M9 on the basis of the modern calibration were below or near freezing.

## 5. DISCUSSION

The advantages of using *P. staminea* shells as potential geochemical archives were its high growth rate (>1 mm/month), which allowed submonthly time resolution, and its compositional banding, which provided independent information about whether conditions were favorable or unfavorable for shell growth. A disadvantage was that *P. staminea* shell deposition appeared to occasionally stop or slow for more than a day. Geochemical variations in the shell thus might not reflect the full range of environmental variability. For example, the lack of negative shell $\delta^{18}O$ excursions corresponding to winter precipitation and the lack of geochemical variations corresponding to the September–October 1997 El Niño–related temperature rise are difficult to explain unless shell growth stopped or was slow enough to preclude resolution of these events. It is interesting to note that annual bands in Humboldt Bay *P. staminea* shells were deposited in March or April. This differed from *P. staminea* growth patterns at sites with weaker coastal upwelling, where the annual band was deposited in winter.

### 5.1. Environmental and Biologic Influences on *P. staminea* Shell Geochemistry

The comparison of environmental variables and shell geochemistry was complicated by the fact that the Humboldt Bay *P. staminea* shell was not collected live. However, shell growth

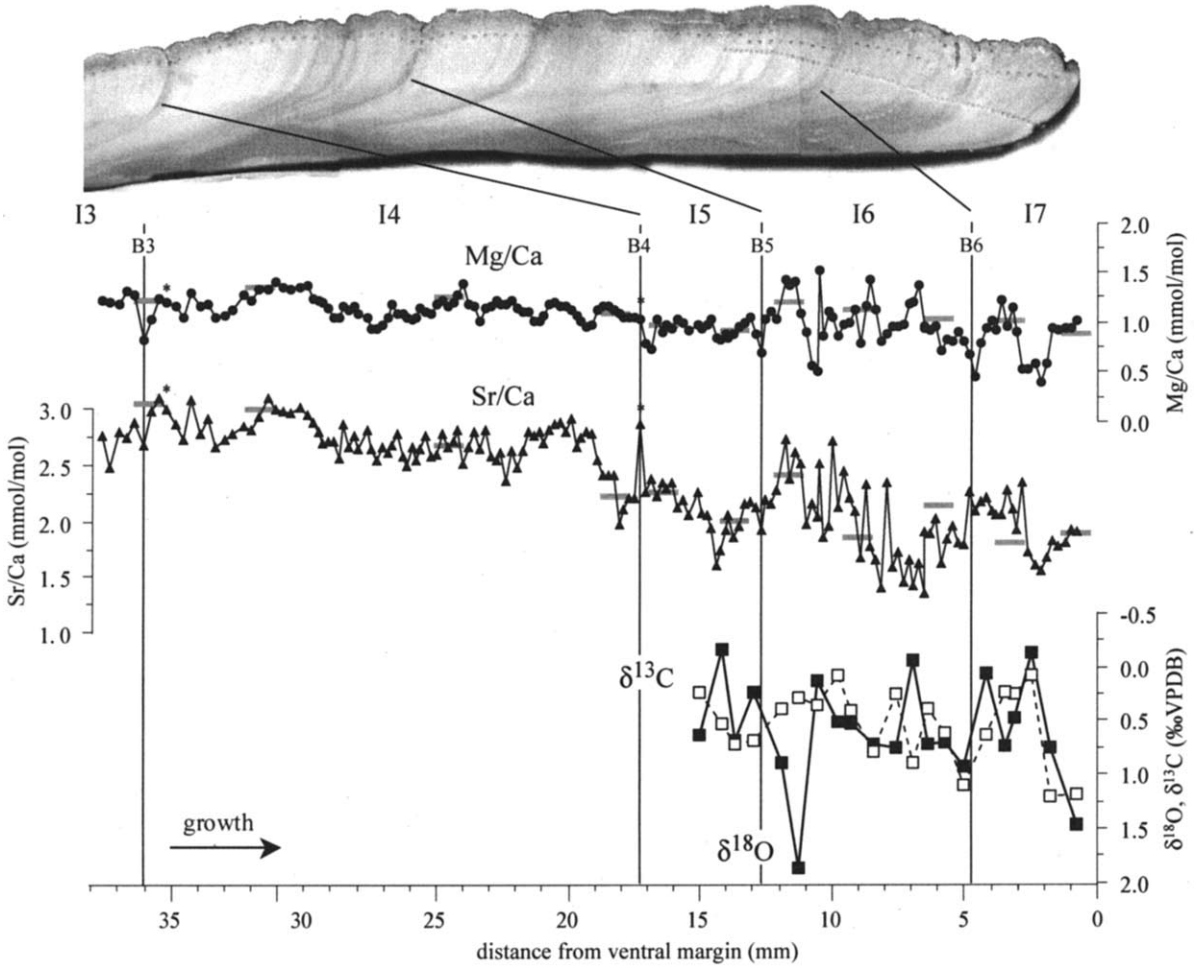


Fig. 9. Cross-sectional photograph and Mg/Ca, Sr/Ca, $\delta^{13}C$, and $\delta^{18}O$ profiles of shell M9 plotted against distance from the ventral margin. Stable isotopes are plotted on a reversed scale to emphasize warm and fresh conditions. Vertical lines show where growth bands (B) separate growth increments (I). Horizontal gray bars on Mg/Ca and Sr/Ca plots show absolute Mg/Ca and Sr/Ca ratios determined by flame atomic absorption. Arrow indicates direction of growth. Asterisks (*) indicate spots with Mn >40 ppm. Laser ablation craters are visible along the upper edge of the shell.

banding and the strong correlation between Mg/Ca and temperature corroborated the placement of I4 in the period March 1996–March 1997, relative to the temperature record that began in October 1993.

### 5.1.1. *Physiologic influences on P. staminea Mg/Ca ratios*

No single environmental variable could account for Mg/Ca variations observed throughout HB1. A strong correlation between Mg/Ca and temperature, similar to that found in the calcite layer of *M. trossulus* (Klein et al., 1996a) and *M. edulis* 50–63 d after transplantation (Vander Putten et al., 2000), was observed in only one of four analyzed growth increments (I4) of the Humboldt Bay *P. staminea* shell. The temperature dependence of Mg incorporation in I4 of HB1, approximately 9 ± 2% (95% confidence interval) increase/1°C increase, was higher than the temperature dependence of Mg incorporation in *M. trossulus* calcite, approximately 5 ± 1% (95% confidence interval) (Klein et al., 1996a). Shell Mg/Ca variations in HB1 were not directly caused by water column Mg/Ca variations, since Humboldt Bay salinity was never low enough (salinity <10) to significantly alter dissolved Mg/Ca ratios (Dodd and Crisp, 1982; Klein et al., 1996a).

In some sections of the shell, it appears that Mg/Ca ratios were related to the proportion of organic matter to calcium carbonate ablated. All but two (B4 in HB1, B4 in M9) organic-rich growth bands in the three *P. staminea* shells were associated with lower Mg/Ca ratios than previously deposited aragonite-rich layers. This suggests that organic layers deposited when shell growth slowed, presumably in response to decreasing temperatures, generally contained less Mg than carbonate-rich layers. Pannella (1975), and other studies referenced therein, reported that organic-rich layers were distinct structurally (more resistant to acid-etching) and chemically (amino acid composition) from the intracrystalline organic matrix. Thus, Mg-depleted organic layers in *P. staminea* might not preclude a Mg-enriched intracrystalline organic matrix, which is indicated by 52% less Mg in shell powder with the organic fraction removed. Our finding that organic-rich layers were

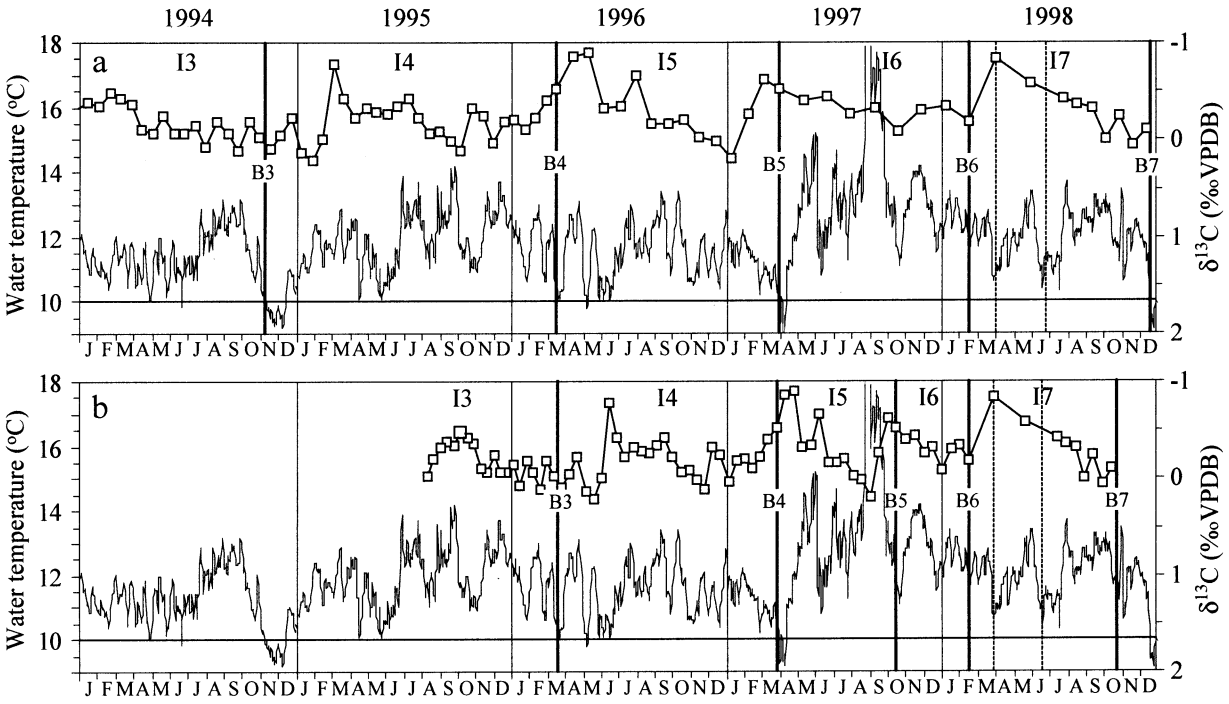


Fig. 10. Versions of the HB1 chronology showing Humboldt Bay water temperature during 1994–1998 (fine line) and shell $\delta^{13}C$ (open squares). Horizontal line indicates 10°C. Thick vertical lines indicate growth bands (B) separating growth increments (I). Dashed vertical lines in I7 indicate positions of growth checks. Timescales were determined iteratively assuming a) that B6 was deposited in February 1998 and that growth bands formed annually during the first occurrence of temperatures near 10°C, and b) that I6 represented ~4 months of growth and the growth rate in I7 after the second growth check was similar to that in I4.

depleted in Mg was opposite to that of Rosenberg et al. (2001) who showed that the Mg content of *Mytilus* sp. calcite was higher in slower-growing, organic-rich, more metabolically active regions of the ventral margin. It is not certain, however, whether Rosenberg's metabolic model of Mg incorporation in shell calcite would apply to shell aragonite, which has a crystal lattice that does not favor Mg incorporation. It is also uncertain whether the relationship between Mg incorporation and mantle metabolic activity at different positions along the shell margin would apply to Mg incorporation as metabolic activity changed through time at one position along the shell margin.

### 5.1.2. *Influence of growth rate on P. staminea Sr/Ca ratios*

Assuming that growth lines corresponding to lunar days were correctly identified in I7 of HB1, the coincidence of highest Sr/Ca ratios with widely spaced growth lines and decreasing Sr/Ca ratios with narrowing growth lines suggests a positive correlation between growth rate and Sr incorporation in aragonitic *P. staminea* shells. Growth rate-dependent Sr incorporation would be consistent with Sr/Ca patterns at the ends of I3 and I4, where Sr/Ca ratios began to increase after the first short-lived upwelling events of 1996 and 1997, which presumably led to increased food availability for *P. staminea.* Thus, apparent correlations between shell Sr/Ca ratios and water temperatures in I4 and I6 probably reflect increased shell growth rate at higher temperatures. The ontogenetic trend of decreasing mean Sr/Ca ratios in HB1 is also consistent with growth rate-dependent Sr incorporation, since *P. staminea* growth rate decreases with age.

### 5.1.3. *Effects of estuarine salinity and temperature on P. staminea $\delta^{18}O$*

If the relation between salinity and $\delta^{18}O_{water}$ reported by Ingram et al. (1996) for San Francisco Bay is applicable, then $\delta^{18}O$ values of Humboldt Bay waters would have ranged from −2.7‰ to 0.8‰ (VSMOW, Vienna Standard Mean Ocean Water) for salinities ranging from 25.8 to 36.7 in 1995–1998. Using the equation of Grossman and Ku (1986) to account for temperature-dependent $^{18}O/^{16}O$ fractionation in aragonitic mollusc shells, HB1 would be expected to have $\delta^{18}O$ values ranging from −0.6‰ to 2.9‰ (Fig. 11) with a mode of 1.8‰ during upwelling months, reflecting stable environmental conditions. During rainy seasons, measured shell $\delta^{18}O$ were in reasonable agreement with the most negative predicted $\delta^{18}O$ values
(Fig. 11). The 0.3‰ higher-than-predicted shell $\delta^{18}O$ values in April 1996 and at the height of the El Niño storm season in February 1998 could be accounted for by a 1-unit salinity increase. During summer upwelling seasons, in contrast, the $\delta^{18}O$ mode value was more than 1‰ lower than predicted (Fig. 11). This might reflect differences in water temperatures over the King Salmon mudflat and at the Coast Guard (CG) pier, where HB water temperatures were measured. Water temper-

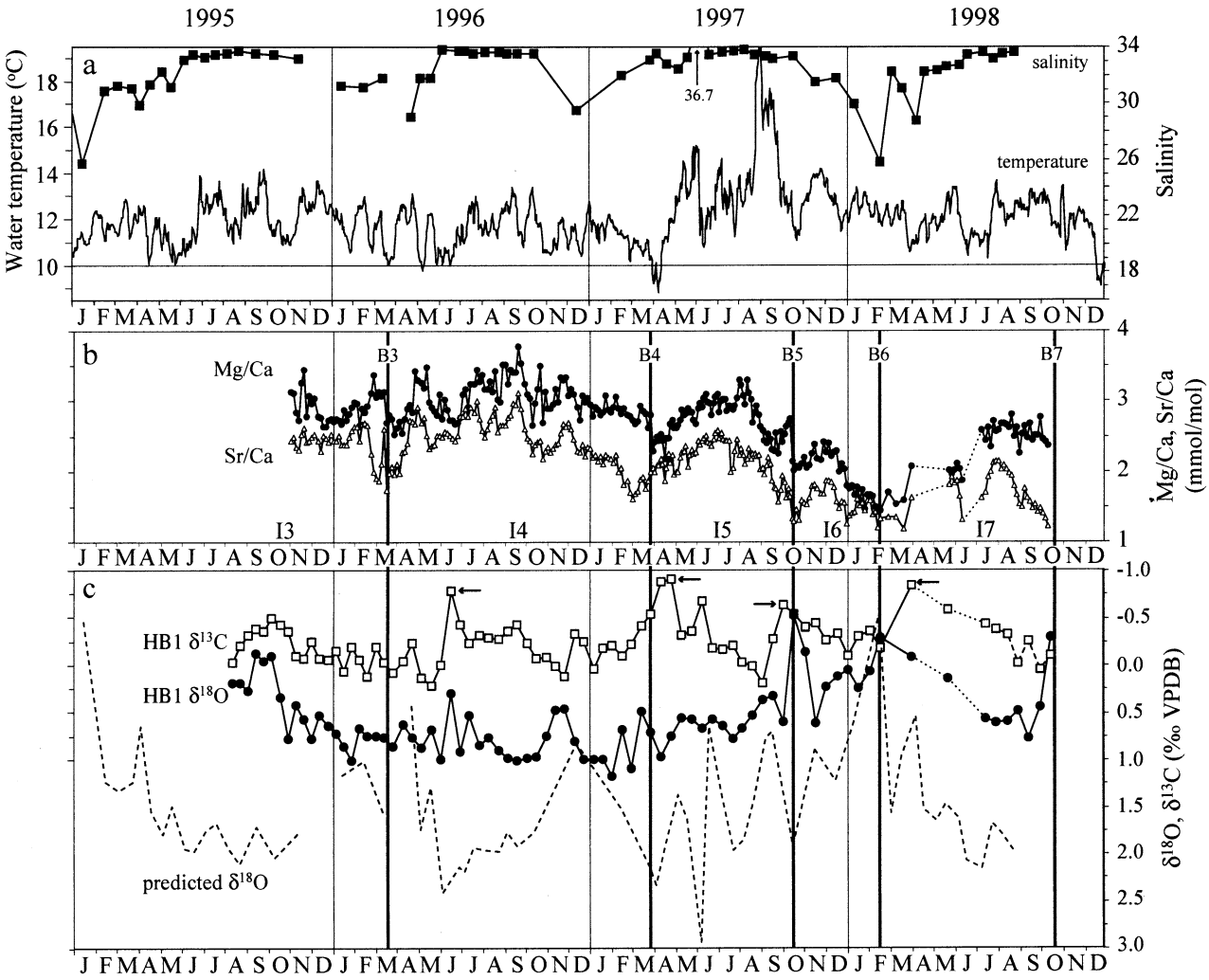


Fig. 11. Comparisons of a) Humboldt Bay salinity and temperature during 1995–1998 to b) HB1 Mg/Ca and Sr/Ca ratios, and c) HB1 $\delta^{13}C$ and $\delta^{18}O$ (reversed scale) plotted using the final chronology. Predicted shell $\delta^{18}O$ values, found using ambient temperature, salinity, and the equations of Ingram et al. (1996) and Grossman and Ku (1986), are also shown in (c). Horizontal line on the temperature plot indicates 10°C. Thick vertical lines indicate positions of growth bands (B). (I) indicates growth increments. Dotted lines on Mg/Ca, Sr/Ca, $\delta^{13}C$, and $\delta^{18}O$ plots show inferred growth hiatuses. Arrows pointing to $\delta^{13}C < -0.5‰$ show coastal upwelling events.

atures in shallow northern reaches of Humboldt Bay may reach 20°C (Barnhart et al., 1992), so it seems possible that water temperatures over the shallow King Salmon mudflat were several degrees warmer than indicated by the temperature sensor. If temperatures over the King Salmon mudflat were 4.5°C higher than at the CG pier, measured shell $\delta^{18}O$ would be in agreement with predicted $\delta^{18}O$. Since measured *P. staminea* shell $\delta^{18}O$ values were similar to those predicted from thermodynamic equilibrium in winter, it does not seem likely that offsets between predicted and observed shell $\delta^{18}O$ in summer and fall can be explained by aragonite precipitation out of oxygen isotope equilibrium with ambient water.

### *5.1.4. Effects of coastal upwelling on P. staminea $\delta^{13}C$*

The abrupt occurrence of shell $\delta^{13}C$ values less than $-0.5‰$ and their coincidence with salinity >33, as well as reduced water temperatures, suggests that the most negative $\delta^{13}C$ values in I4, I5, and I6 of HB1 resulted from coastal upwelling events. In the California Current at 42°N, waters upwelled from 200 m depth would be expected to have a $\delta^{13}C_{DIC}$ value 1.8‰ lower than surface waters (Ortiz et al., 2000). This was twice the $\delta^{13}C$ range observed within any increment of HB1. However, surface water runoff containing $^{12}C$-rich terrestrially derived carbon in winter and spring could have decreased annual $\delta^{13}C_{DIC}$ ranges in HB compared to that of the coastal ocean. It also seems likely that $^{12}C$-rich metabolically derived carbon was incorporated into HB1 aragonite, since shell $\delta^{13}C$ values were over 2‰ lower than expected during upwelling according to the $\delta^{13}C_{aragonite}$-temperature relation found by Grossman and Ku (1986) for molluscs. The 2‰ difference was calculated assuming a water temperature of 10.5°C and water column $\delta^{13}C_{DIC} = 0.1‰$ during upwelling (Ortiz et al., 2000). Follow-

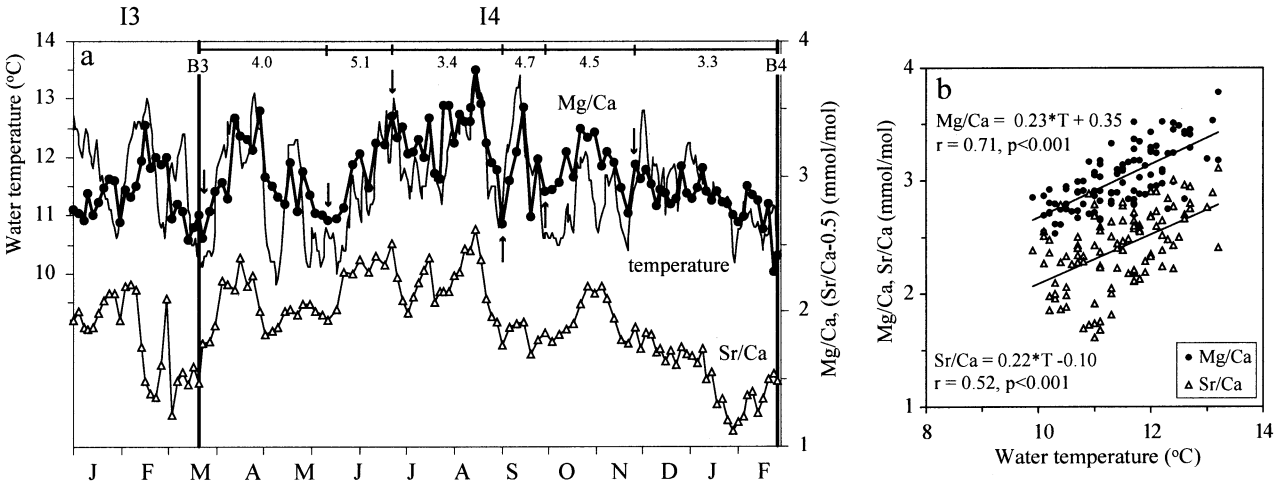


Fig. 12. a) Mg/Ca ratios (filled circles) plotted with daily water temperatures (fine line) using the fine-tuned timescale in I4. Vertical lines indicate positions of growth bands (B3, B4). Arrows and divided bar at top indicate tie-points between Mg/Ca and temperature records, and B4 is also a tie point. Numbers at top indicate the number of days between laser spots when tie-points were used. Before fine-tuning there were 3.8 d between laser spots. Sr/Ca ratios (open triangles), shown for comparison, were scaled by −0.5 mmol/mol to plot on the Mg/Ca scale. b) Linear least-squares fits to I4 Mg/Ca and Sr/Ca regressed against temperature (T). Correlation coefficients, r, and levels of significance, p, are given for both regressions.

ing upwelling events, gradually increasing shell $\delta^{13}C$ values were consistent with increasing primary productivity and $^{13}C$ enrichment of Humboldt Bay surface waters.

### 5.2. Paleoenvironmental Interpretations

Despite poor physical preservation of M3, its primary aragonite mineralogy, manganese concentrations <10 ppm, and seawater-like $\delta^{18}O$ values indicate that it did not undergo extensive diagenetic alteration. Cyclic Mg/Ca variations in I8, I9, and I10 suggest the local environment was controlled by a highly seasonal processes, possibly solar heating. High positive $\delta^{13}C$ values in M3 suggest the shell precipitated in $^{12}C$-depleted waters, possibly highly productive or stratified surface waters (Grossman, 1984; Purton and Brasier, 1997; Hendry et al., 2001). The absence of geochemical and microstructural features associated with upwelling, such as negative $\delta^{13}C$ values or mid-increment organic-rich layers, may also indicate that shell M3 grew in an environment that was stratified in summer. Considered as whole, the evidence suggests that ~3000 yr-old *P. staminea* shell grew in a low energy environment such as a protected embayment or lagoon (Krantz et al., 1987; Bemis and Geary, 1996; Purton and Brasier, 1997; Hendry et al., 2001). While paleofaunal analyses suggest that rocky intertidal habitat dominated the coast around this time, a low ratio of burrowing to rock-perching bivalve shells in the midden does not preclude the existence of a coastal embayment.

Gaffey et al. (1991) found that roasting at 200°C had no effect on skeletal aragonite Mg and Sr contents. Wood fires burn at temperatures between 200–250°C, so even if shell M9 was cooked, this would not have significantly altered Mg and Sr contents. Neither did M9 undergo major diagenetic alteration, since the shell was composed of primary aragonite and oxygen and carbon do not appear to have exchanged with meteoric water. However, relatively elevated Mn throughout M9 could be evidence that Ca-substituting ions in the aragonite lattice, i.e., Mg and Sr, exchanged with meteoric water. In addition, organically complexed Mg may have been lost as the intracrystalline organic matrix degraded over time (Curtis and Krinsley, 1965). Despite these limitations, high positive $\delta^{18}O$ values near annual growth bands in M9 appear to indicate cooler winters than today. This would be consistent with lower solar insolation (Kutzbach et al., 1998) and with radiolarian-based transfer functions from ODP Site 1019 corresponding to lower mean sea surface temperatures in the early Holocene (Pisias et al., 2001).

## 6. CONCLUSIONS

Despite generally high growth rates, *P. staminea* shells are not ideal geochemical archives because they contain growth hiatuses that appear to exclude extreme events. This could in part explain why only one growth increment in a modern *P. staminea* specimen from Humboldt Bay, California, showed a systematic relationship between temperature and Mg/Ca. Qualitatively, Sr/Ca ratios appeared to depend on shell growth rate.

A more promising environmental indicator in the Humboldt Bay *P. staminea* shell appears to be its carbon isotope composition, which records spring and summer coastal upwelling events. Reconstructions of past coastal upwelling might be possible using shell $\delta^{13}C$ and another coastal upwelling proxy, such as Cd/Ca, which is not metabolically sensitive.

The original Mg content of *P. staminea* shells deposited ~3000 and ~9000 yr ago does not appear to have been preserved, possibly because organically complexed Mg, which is a significant fraction of total Mg, was lost. Nevertheless, relative Mg/Ca variations within the ~3000-yr-old shell appear to reflect variations in ambient temperature. High positive $\delta^{13}C$ values in the ~3000-yr-old shell suggest it grew in a low-energy environment such as a protected embayment or lagoon.

High positive $\delta^{18}O$ values in the ~9000-yr-old shell suggest cooler winters than today in the early Holocene.

*Acknowledgments*—Holocene-age mollusc shells from the Duncan's Landing Cave site were obtained from the California Department of Parks and Recreation Cultural Heritage Section. We thank Shad Baiz, Michelle Large, and John Hill for collecting and processing Humboldt Bay water samples. Some funding for this work was provided by the Columbia University Department of Earth and Environmental Sciences and by the Lamont-Doherty Earth Observatory Climate Center. The authors thank Louise M. A. Hildebrand (née Purton) and two anonymous reviewers for suggestions that improved the manuscript. This is LDEO contribution 6590.

*Associate editor:* D. W. Lea

## REFERENCES

Bakun A. (1990) Global climate change and intensification of coastal ocean upwelling. *Science* **247**(4939), 198–201.

Bard E., Hamelin B., Fairbanks R. G., and Zindler A. (1990) Calibration of the $^{14}C$ timescale over the past 30,000 years using mass spectrometric U-Th ages from Barbados corals. *Nature* **345,** 405–410.

Barnhart R. A., Boyd M. J., and Pequegnat J. E. (1992) *The Ecology of Humboldt Bay, California: An Estuarine Profile.* U.S. Fish and Wildlife Service.

Basil A. and Bush G. (2001) Pacific sea surface temperature forcing dominates orbital forcing of the Early Holocene monsoon. *Quat. Res.* **55**(1), 25–32.

Bemis B. E. and Geary D. H. (1996) The usefulness of bivalve stable isotope profiles as environmental indicators: Data from the eastern Pacific Ocean and the southern Caribbean sea. *Palaios* **11**(4), 328–339.

Berry W. B. N. and Barker R. M. (1975) Growth increments in fossil and modern bivalves. In *Growth Rhythms and the History of the Earth's Rotation* (eds. G. C. Rosenberg and S. K. Runcorn), p. 559. Wiley.

Brand U. and Veizer J. (1980) Chemical diagenesis of a multicomponent carbonate system 1: Trace elements. *J. Sediment. Petrol.* **50**(4), 1219–1236.

Brink K. H. and Cowles T. J. (1991) The coastal transition zone program. *J. Geophys. Res.* **96**(C8), 14637–14647.

Chavez F. P. and Toggweiler J. R. (1995) Physical estimates of global new production: The upwelling contribution. In *Upwelling in the Ocean: Modern Processes and Ancient Records*, Vol. 18 (eds. C. P. Summerhayes, K.-C. Emeis, M. V. Angel, R. L. Smith, and B. Zeitzschel), pp. 337–360. Wiley.

Curtis C. D. and Krinsley D. (1965) The detection of minor diagenetic alteration in shell material. *Geochim. Cosmochim. Acta* **29**(1), 71–84.

Dodd J. R. (1965) Environmental control of strontium and magnesium in *Mytilus. Geochim. Cosmochim. Acta* **29**(5), 385.

Dodd J. R. (1967) Magnesium and strontium in calcareous skeletons: A review. *J. Paleontol.* **41**(6), 1313–1329.

Dodd J. R. and Crisp E. L. (1982) Non-linear variation with salinity of Sr/Ca and Mg/Ca ratios in water and aragonitic bivalve shells and implications for paleosalinity studies. *Paleogeogr. Paleoclimatol. Paleoecol.* **38**(1–2), 45–56.

Drever J. I. (1997) *The Geochemistry of Natural Waters, Surface and Groundwater Environments.* Prentice-Hall.

Edwards R. L., Beck J. W., Burr G. S., Donahue D. J., Chappell J. M., Bloom A. L., Druffel E. R. M., and Taylor F. W. (1993) A large drop in atmospheric $^{14}C/^{12}C$ and reduced melting in the Younger Dryas, documented with $^{230}Th$ ages of corals. *Science* **260,** 962–968.

Eisma D., Mook W. G., and Das H. A. (1976) Shell characteristics, isotopic composition, and trace-element contents of some euryhaline molluscs as indicators of salinity. *Paleogeogr. Paleoclimatol. Paleoecol.* **19,** 39–62.

Emiliani C. (1955) Pleistocene temperatures. *J. Geol.* **63,** 538–578.

Epstein S., Buchsbaum R., Lowenstam H. A., and Urey H. C. (1953) Revised carbonate-water isotopic temperature scale. *Geol. Soc. Am. Bull.* **64,** 1315–1326.

Erlandson J. (1994) *Early Hunter-Gatherers of the California Coast.* Plenum Press.

Evans J. W. (1972) Tidal growth increments in the cockle *Clinocardium nuttalli. Science* **176,** 416–417.

Fallon S. J., White J. C., and McCulloch M. T. (2002) *Porites* corals as recorders of mining and environmental impacts: Misima Island, Papua New Guinea. *Geochim. Cosmochim. Acta* **66**(1), 45–62.

Feder H. M., Hendee J. C., Holmes P., Mueller G. J., and Paul A. J. (1979) Examination of a reproductive cycle of *Protothaca staminea* using histology, we weight-dry weight ratios, and condition indices. *Veliger* **22**(2), 182–187.

Feng R. (1994) In situ trace element determination of carbonates by LaserProbe inductively coupled plasma mass spectrometry using nonmatrix matched standardization. *Geochim. Cosmochim. Acta* **58**(6), 1615–1623.

Fraser C. M. and Smith G. M. (1928) Notes on the ecology of the little neck clam. *Paphia staminea Conrad. Trans. R. Soc. Can. Ser.* **3,** 249–269.

Fuge R., Palmer T. J., Pearce N. J. G., and Perkins W. T. (1993) Minor and trace element chemistry of modern shells: A laser ablation inductively coupled plasma mass spectrometry study. *Appl. Geochem.* **2**(Suppl.), 111–116.

Gaffey S. J., Kolak J. J., and Bronnimann C. E. (1991) Effects of drying, heating, annealing, and roasting of carbonate skeletal material, with geochemical and diagenetic implications. *Geochim. Cosmochim. Acta* **55,** 1627–1640.

Grossman E. L. (1984) Stable isotope fractionation in live benthic foraminifera from the southern California Borderland. *Paleogeogr. Paleoclimatol. Paleoecol.* **47,** 301–327.

Grossman E. L. and Ku T. (1986) Oxygen and carbon isotope fractionation in biogenic aragonite: Temperature effects. *Chem. Geol.* **59,** 59–74.

Harrington R. J. (1985) Growth patterns within the genus *Protothaca* (Bivalvia: Veneridae) from the Gulf of Alaska to Panama: Paleotemperatures, paleobiogeography and paleolatitudes. Ph.D. thesis. University of California Santa Barbara.

Harrington R. J. (1987) Skeletal growth histories of *Protothaca staminea* (Conrad) and *Protothaca grata* (Say) throughout their geographic ranges, Northeastern Pacific. *Veliger* **30**(2), 148–158.

Hendry J. P., Perkins W. T., and Bane T. (2001) Short-term environmental change in a Jurassic lagoon deduced from geochemical trends in aragonite bivalve shells. *Geol. Soc. Am. Bull.* **113**(6), 790–798.

Huyer A. (1983) Coastal Upwelling in the California Current System. *Prog. Oceanogr.* **12**(3), 259–284.

Ingram B. L., Conrad M. E., and Ingle J. C. (1996) Stable isotope and salinity systematics in estuarine waters and carbonates: San Francisco Bay. *Geochim. Cosmochim. Acta* **60**(3), 455–467.

Jones D. S. and Allmon W. D. (1995) Records of upwelling, seasonality and growth in stable-isotope profiles of Pliocene mollusk shells from Florida. *Lethaia* **28,** 61–74.

Kennish M. J. (1980) Shell microgrowth analysis: *Mercenaria mercenaria* as a type example for research in population dynamics. In *Skeletal Growth of Aquatic Organisms: Biological Records of Environmental Change*, Vol. 1 (eds. D. C. Rhoads and R. A. Lutz), pp. 255–294. Plenum.

Killingley J. S. and Berger W. H. (1979) Stable isotopes in a mollusc shell: Detection of upwelling events. *Science* **205,** 186–188.

Klein R. T., Lohmann K. C., and Thayer C. W. (1996a) Bivalve skeletons record sea-surface temperature and $\delta^{18}O$ via Mg/Ca and $^{18}O/^{16}O$ ratios. *Geology* **24**(5), 415–418.

Klein R. T., Lohmann K. C., and Thayer C. W. (1996b) Sr/Ca and $^{13}C/^{12}C$ ratios in skeletal calcite of *Mytilus trossulus:* Covariation with metabolic rate, salinity, and carbon isotopic composition of seawater. *Geochim. Cosmochim. Acta* **60**(21), 4207–4221.

Krantz D. E. (1990) Mollusk-isotope records of Plio-Pleistocene marine paleoclimate, U.S. Middle Altantic Coastal Plain. *Palaios* **5,** 317–335.

Krantz D. E., Williams D. F., and Jones D. S. (1987) Ecological and paleoenvironmental information using stable isotope profiles from

living and fossil mollusks. *Paleogeogr. Paleoclimatol. Paleoecol.* **58**(3–4), 249–266.

Krantz D. E., Kronick A. T., and Williams D. F. (1988) A model for interpreting continental-shelf hydrographic processes from the stable isotope and cadmium–calcium profiles of scallop shells. *Paleogeogr. Paleoclimatol. Paleoecol.* **64**(3–4), 123–140.

Kutzbach J. E. and Ruddiman W. F. (1993) Model description, external forcing, and surface boundary conditions. In *Global Climates since the Last Glacial Maximum* (eds. H. E. Wright Jr., J. E. Kutzbach, T. Webb III, W. F. Ruddiman, F. A. Street-Perrott, and P. J. Bartlein), pp. 12–23. University of Minnesota Press.

Kutzbach J., Gallimore R., Harrison S., Behling P., Selin R., and Laarif F. (1998) Climate and biome simulations for the past 21,000 years. *Quat. Sci. Rev.* **17**(6–7), 473–506.

Land L. S. (1967) Diagenesis of skeletal carbonates. *J. Sediment. Petrol.* **37**(3), 914–930.

Mook W. G. (1970) Stable carbon and oxygen isotopes of natural waters in the Netherlands. In *Isotope Hydrology*, pp. 163–190. IAEA.

Mook W. G. and Vogel J. C. (1968) Isotopic equilibrium between shells and their environment. *Science* **159,** 874–875.

Ortiz J. D., Mix A. C., Wheeler P. A., and Key R. M. (2000) Anthropogenic $CO_2$ invasion into the northeast. Pacific based on concurrent $\delta^{13}C_{DIC}$ and nutrient profiles from the California Current. *Glob. Biogeochem. Cycle* **14**(3), 917–929.

Pannella G. (1975) Palaeontological clocks and the history of the Earth's rotation. In *Growth Rhythms and the History of the Earth's Rotation* (eds. G. D. Rosenberg and S. K. Runcorn), pp. 253–284. Wiley.

Paul A. J. and Feder H. M. (1973) Growth, recruitment, and distribution of the littleneck clam *Protothaca staminea*, in Galena Bay, Prince William Sound, Alaska. *Fish. Bull.* **71**(3), 665–677.

Perkins W. T., Fuge R., and Pearce N. J. G. (1991) Quantitative analysis of trace elements in carbonates using laser ablation inductively-coupled plasma mass-spectrometry. *J. Anal. Atom. Spectrom.* **6**(6), 445–449.

Peterson C. H. and Ambrose W. G. Jr. (1985) Potential habitat dependence in deposition of presumptive annual lines in shells of the bivalve *Protothaca staminea*. *Lethaia* **18,** 257–260.

Pisias N. G., Mix A. C., and Heusser L. (2001) Millennial scale climate variability of the northeast Pacific Ocean and northwest North America based on radiolaria and pollen. *Quat. Sci. Rev.* **20**(14), 1561–1576.

Purton L. and Brasier M. (1997) Gastropod carbonate $\delta^{18}O$ and $\delta^{13}C$ values record strong seasonal productivity and stratification shifts during the late Eocene in England. *Geology* **25**(10), 871–874.

Purton L. M. A., Shields G. A., Brasier M. D., and Grime G. W. (1999) Metabolism controls Sr/Ca ratios in fossil aragonitic mollusks. *Geology* **27**(12), 1083–1086.

Quayle D. B. (1943) Sex, gonad development, and seasonal gonad changes in *Paphia staminea* Conrad. *J. Fish. Res. Bd. Can.* **6**(2), 140–151.

Rhoads D. C. and Lutz R. A. (1980) *Skeletal Growth of Aquatic Organisms*: *Biological Records of Environmental Change*. Plenum.

Rosenberg G. D. and Hughes W. W. (1991) A metabolic model for the determination of shell composition in the bivalve mollusk. *Mytilus edulis. Lethaia* **24**(1), 83–96.

Rosenberg G. D., Hughes W. W., Parker D. L., and Ray B. D. (2001) The geometry of bivalve shell chemistry and mantle metabolism. *Am. Malacol. Bull.* **16**(1–2), 251–261.

Rosenthal Y., Field M. P., and Sherrell R. M. (1999) Precise determination of element/calcium ratios in calcareous samples using sector field inductively coupled plasma mass spectrometry. *Anal. Chem.* **71**(15), 3248–3253.

Ryan H., Gibbons H., Hendley II J. W., and Stauffer P. (1999) El Niño sea-level rise wreaks havoc in California's San Francisco Bay region, p. 4. U.S. Geological Survey Fact Sheet 175-99.

Schmidt R. R. and Warme J. E. (1969) Population characteristics of *Protothaca staminea* (Conrad) from Mugu Lagoon, California. *Veliger* **12**(2), 193–199.

Schrag D. P., Hampt G., and Murray D. W. (1996) Pore fluid constraints on the temperature and oxygen isotopic composition of the glacial ocean. *Science* **272,** 1930–1932.

Schwing F. B., O'Farrell M., Steger J., and Baltz K. (1996) Coastal upwelling indices, west coast of North America, 1946–1995. NOAA Technical Memorandum.

Schwing F. B. and Mendelssohn R. (1997) Increased coastal upwelling in the California Current System. *J. Geophys. Res.* **102**(C2), 3421–3438.

Schwing F. B., Murphree T., deWitt L., and Green P. M. (2002) The evolution of oceanic and atmospheric anomalies in the northeast Pacific during the El Niño and La Niña events of 1995–2001. *Prog. Oceanogr.* **54**(1–4), July–Sept.

Sinclair D. J., Kinsley L. P. J., and McCulloch M. T. (1998) High resolution analysis of trace elements in corals by laser ablation ICP-MS. *Geochim. Cosmochim. Acta* **62**(11), 1889–1901.

Smith G. M. (1928) Food material as a factor in growth rate of some Pacific clams. *Trans. R. Soc. Can. Ser.* **3**287–291.

Stecher H. A., Krantz D. E., Lord C. J., Luther G. W., and Bock K. W. (1996) Profiles of strontium and barium in *Mercenaria mercenaria* and *Spisula solidissima* shells. *Geochim. Cosmochim. Acta* **60**(18), 3445–3456.

Sylvester P. J. and Ghaderi M. (1997) Trace element analysis of scheelite by excimer laser ablation inductively coupled plasma mass spectrometry (ELA-ICP-MS) using a synthetic silicate glass standard. *Chem. Geol.* **141**(1–2), 49–65.

Tanaka N., Monaghan M. C., and Rye D. M. (1986) Contribution of metabolic carbon to mollusc shell carbonate. *Nature* **320,** 520–523.

Toland H., Perkins B., Pearce N., Keenan F., and Leng M. J. (2000) A study of sclerochronology by laser ablation ICP-MS. *J. Anal. Atom. Spectrom.* **15**(9), 1143–1148.

UNESCO. (1981) The practical salinity scale 1978 and the international equation of state of seawater 1980. In *UNESCO Technical Papers in Marine Science*, Vol. 36, p. 25. UNESCO Division of Marine Sciences.

van Geen A., Takesue R. K., Goddard J., Takahashi T., Barth J. A., Smith R. L. (2000) Carbon and nutrient dynamics during coastal upwelling off Cape Blanco, Oregon. *Deep Sea Res. II* **47**(5–6), 975–1002.

Vander Putten E., Dehairs F., Keppens E., and Baeyens W. (2000) High resolution distribution of trace elements in the calcite shell layer of modern *Mytilus edulis*: Environmental and biological controls. *Geochim. Cosmochim. Acta* **64**(6), 997–1011.

Wolf K. H., Chilingar G. V., and Beales F. W. (1967) Elemental composition of carbonate skeletons, minerals and sediments. In *Carbonate Rocks, Physical and Chemical Aspects*, Vol. 9B (ed. G. V. Chilingar), pp. 23–151. Elsevier.